

New conductive filament ready-to-use for 3D-printing electrochemical (bio)sensors: Towards the detection of SARS-CoV-2

Jéssica Santos Stefano^{a,*}, Luiz Ricardo Guterres e Silva^a, Raquel Gomes Rocha^b, Laís Canniatti Brazaca^{c,d}, Eduardo Mathias Richter^{b,d}, Rodrigo Alejandro Abarza Muñoz^{b,d*}, Bruno Campos Janegitz^{a*}

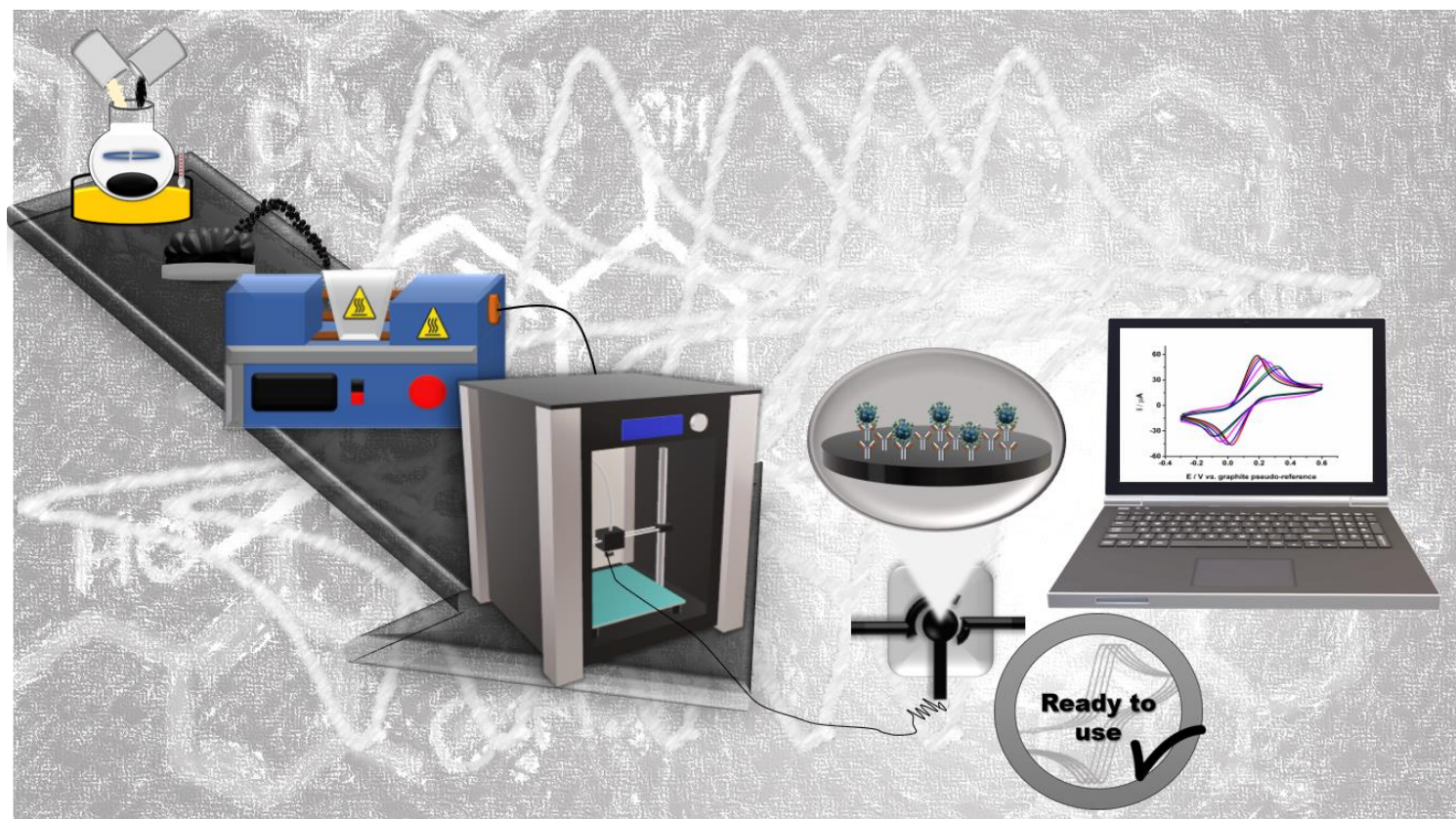
^aDepartment of Nature Sciences, Mathematics and Education, Federal University of São Carlos, 13600-970, Araras, São Paulo, Brazil

^bInstitute of Chemistry, Federal University of Uberlândia, 38400-902, Uberlândia, Minas Gerais, Brazil

^cNanomedicine and Nanotoxicology Group, São Carlos Institute of Physics, University of São Paulo, 13560-970, São Carlos, São Paulo, Brazil

^dNational Institute of Science and Technology in Bioanalysis-INCTBio, 13083-970, Campinas, São Paulo, Brazil

***Corresponding authors: munoz@ufu.br,
jessica.s.stefano@gmail.com
brunocj@ufscar.br**



Abstract

The 3D printing technology has gained ground due to its wide range of applicability. The development of new conductive filaments contributes significantly to the production of improved electrochemical devices. In this context, we report a simple method to producing an efficient conductive filament, containing graphite within the polymer matrix of PLA, and applied in conjunction with 3D printing technology to generate (bio)sensors without the need for surface activation. The proposed method for producing the conductive filament consists of four steps: (i) mixing graphite and PLA in a heated reflux system; (ii) recrystallization of the composite; (iii) drying and; (iv) extrusion. The produced filament was used for the manufacture of electrochemical 3D printed sensors. The filament and sensor were characterized by physicochemical techniques, such as SEM, TGA, Raman, FTIR as well as electrochemical techniques (EIS and CV). Finally, as a proof-of-concept, the fabricated 3D-printed sensor was applied for the determination of uric acid and dopamine in synthetic urine and used as a platform for the development of a biosensor for the detection of SARS-CoV-2. The developed sensors, without pre-treatment, provided linear ranges of 0.5 to 150.0 and 5.0 to 50.0 $\mu\text{mol L}^{-1}$, with low LOD values (0.07 and 0.11 $\mu\text{mol L}^{-1}$), for uric acid and dopamine, respectively. The developed biosensor successfully detected SARS-CoV-2 S protein, with a linear range from 5.0 to 75.0 nmol L^{-1} (0.38 $\mu\text{g mL}^{-1}$ to 5.74 $\mu\text{g mL}^{-1}$) and LOD of 1.36 nmol L^{-1} (0.10 $\mu\text{g mL}^{-1}$) and sensitivity of 0.17 $\mu\text{A nmol}^{-1} \text{L}$ (0.01 $\mu\text{A } \mu\text{g}^{-1} \text{mL}$). Therefore, the lab-made produced and the ready-to-use conductive filament is promising and can become an alternative route for the production of different 3D electrochemical (bio)sensors and other types of conductive devices by 3D printing.

Keywords: Lab-made conductive filament; graphite; PLA, 3D printing; COVID-19 diagnosis.

1. Introduction

Over recent years, technologies based on 3D printing or additive manufacturing have received significant attention, which can facilitate customized fabrication and provide fast and low-cost production of complex three-dimensional devices [1,2]. This emerging technology has been used for numerous applications in different areas, such as healthcare, engineering, pharmaceutical, chemistry, and electrochemistry [2,3]. Electrochemistry and analytical chemistry are highlighted among the areas that have been benefited by 3D printing with applications to energy storage devices, energy conversion (water splitting), and electrochemical sensors [1,4,5].

The most popular 3D printing technology is via fused deposition modeling (FDM), in which thermoplastic filaments are extruded to create layer-by-layer three-dimensional structures. For the development of electrochemical sensors, the use of conductive filaments based on a mix of conductive materials and polymers has become extremely advantageous. In this context, graphene and carbon black-based conductive filaments have been extensively studied due to the low cost, high surface area, good electrical conductivity, and commercial filaments containing these materials were developed (Black magic[®] which is a PLA filament containing graphene, and Proto pasta[®] which is a PLA filament containing carbon black) [6–10]. In addition, other conductive materials can also be employed in the production of 3D printed sensors, such as carbon nanotubes and carbon nanofibers [11–14]. However, the electrochemical response of the as printed electrodes is relatively poor if compared to other carbonaceous surfaces (glassy carbon, carbon paste, etc.). In this regard, some works in the literature have highlighted the need for pre-treatments (activations) or modification of the 3D printed surface electrodes to reduce the amount of insulating polymer, obtaining greater exposition of the conductive material, or increasing the porosity of the

3D printed electrodes, consequently, a significant improvement in the electron transfer kinetics of the 3D printed electrodes and better performance of the electrochemical sensor are observed [5,6,15–17].

Several strategies have been proposed to increase the electrochemical activity of the 3D printed surfaces, such as mechanical polishing [18], electrochemical activation [19], immersion in solvents [16,19], physical methods of thermal annealing [5], biological digestion using enzymes [20], water electrolysis generating hydroxide, and chemical/electrochemical activations [15,21].

Activation procedures may cause the destruction or disintegration of the electrodes, are time-consuming, can generate chemical residues, and its performance depends on the polymeric composition of the filament (or 3D-printed device) [22]. In this aspect, the obtainment of a dispositive that brings the advantages of 3D printing, but provides satisfactory electrochemical responses without the need for surface pre-treatments, saving time and reagents expenditure (environmentally friendly), is emerged as very attractive.

In this context, some authors have been investigating the manufacture of conductive filaments for 3D printing [23,24]. Foster *et al.* proposed the production of filaments containing nanographite (25% wt.) within PLA. The electrochemical performance of the 3D printed electrodes was evaluated for a range of redox probes and the simultaneous detection of lead(II) and cadmium; however, the electrochemical properties were not satisfactory when compared with commercial conductive filaments. Moreover, the procedure involves the use of toxic organic solvents (xylene) and is time-consuming (6 h). Other procedures for the production of filaments to 3D print electrochemical devices were reported in a review [1], however, all of them required surface treatment for improved electrochemical performance.

In this sense, herein we report a simple protocol for the production and characterization (physical and electrochemical) of a new conductive filament containing graphite within the polymer matrix of PLA that is compatible with FDM 3D printing technology to create improved electrochemical (bio)sensors, importantly not requiring surface activation (ready-to-use devices). To the best of our knowledge, this is the first study that shows the manufacture of 3D printed devices without the need for surface activation procedures, however, demonstrating excellent electrochemical activity towards the typical redox probes. To show the versatility of the filaments and 3D-printed devices, we developed an immunosensor for the diagnosis of COVID-19 (spike protein) based on the fabricated graphite-PLA 3D-printed sensor. As the detection of biomarkers is also an important tool for combating more serious health problems, a sensor for the detection of uric acid (UA), a biomarker for COVID-19, and dopamine (DA), considered as a biomarker for Parkinson's disease, were also developed using the fabricated 3D-printed graphite-PLA platform.

The literature shows that 3D printed electrodes obtained from commercially-available filaments were applied for sensing to biosensing of important molecules, such as glucose [25], hydrogen peroxide [26], 1-naphthol [27], catechol [17], and even virus [28,29]. The development of 3D electrochemical immunosensors is an excellent alternative for the large-scale production of rapid and relatively low-cost tests, suitable for the development of point-of-care devices [30–32]. In this context, 3D printing technology can play an important role in facing the COVID-19 pandemic, which is currently ravaging the world, allowing simple and fast manufacturing of substrates on demand, such as personal protective equipment and medical devices [33,34]. In addition, the development of 3D printed electrochemical biosensors capable of detecting the COVID-19 virus (SARS-CoV-2) can be used as a tool of great assistance in the

rapid testing of patients, providing monitoring of infected people. To our knowledge, only two works employing the use of 3D printed electrodes for the detection of SARS-CoV-2 are currently available in the literature [32,35].

2. Experimental

2.1. Reagents and solutions

All chemicals used in this work were of analytical degree, and the solutions were prepared using deionized water with a resistivity higher than 18.0 M Ω cm from a Milli Q water purification system from Millipore (MA, USA). Potassium chloride (≥ 99 % w/w), ethanol (99.5 % v/v), ferrocenemethanol (97 % w/w), uric acid (99 % w/w), dopamine hydrochloride (99 % w/w), hexaammineruthenium(III) chloride (98 % w/w), N-(3- dimethylaminopropyl)-N'-ethylcarbodiimide hydroxchloride (EDC) (98% w/w) and N-hydroxysuccinimide (NHS) (98% w/w) were purchased from Sigma-Aldrich (St. Louis, USA), acetone (99.5 % v/v) and sodium chloride (99 % w/w) from Synth (Diadema, Brazil), chloroform (99.8 % v/v) from Qhemis (Indaiatuba, Brazil), sodium hydroxide (98 % w/w) and sodium phosphate dibasic (99% w/w) from Dinamica (Indaiatuba, Brazil). Bovine Serum Albumin (BSA) from Fisher Chemical™ (Hampton, EUA), and dibasic potassium phosphate (98% w/w) from Cinetica (Jandira, Brazil)

A 0.1 mol L⁻¹ Britton-Robinson (BR) buffer solution (pH 2.0) was used as a supporting electrolyte for uric acid (UA) detection, as described in the literature [25], and was composed of a mixture of 0.04 mol L⁻¹ boric acid (99.5 % w/w) from Vetec (Rio de Janeiro, Brazil), and acetic (99.7 % v/v) and phosphoric (85 % v/v) acids from Dinamica (Indaiatuba, Brazil). Stock solutions of UA were freshly prepared before the experiments, after dissolution (5.0 mmol L⁻¹) in 0.01 mol L⁻¹ sodium hydroxide, followed by dilution in 0.1 mol L⁻¹ BR buffer (pH 2.0) based on previous work from the

literature [36]. A 0.1 mol L^{-1} phosphate buffer solution (PBS; $\text{pH} = 7.0$) was used for dopamine (DA) detection, following the literature [37]. The stock solution of DA (5.0 mmol L^{-1}) was freshly prepared before experiments by dissolution in PBS. For the construction of the calibration curve, the stock solution was diluted in different concentrations in PBS again.

Synthetic urine was prepared following the literature with adaptations [38], and was composed of a mixture of $170.0 \text{ mmol L}^{-1}$ urea (99 % w/w), 2.5 mmol L^{-1} calcium chloride dihydrate ($\geq 99 \text{ \% w/w}$), 10.0 mmol L^{-1} anhydrous sodium sulfate (99 % w/w), 0.4 mmol L^{-1} uric acid (99 % w/w) and 7.0 mmol L^{-1} creatinine ($\geq 98.5 \text{ \% w/w}$) from Sigma-Aldrich, St. Louis, USA; 1.1 mmol L^{-1} lactic acid (85 % v/v), 2.0 mmol L^{-1} citric acid (99.5 % w/w) and 25.0 mmol L^{-1} ammonium chloride (99.5 % w/w) from Dinamica Química (Indaiatuba, Brazil) and 90.0 mmol L^{-1} sodium chloride (99 % w/w) from Synth (Diadema, Brazil). Sodium hydroxide (0.1 mol L^{-1}) was added (1:1000 v/v) to solubilize the UA, and the final solution was diluted 40 times in BR buffer solution (for UA detection), to adjust the final concentration to the calibration curve, or 10 times in PBS (for DA detection). For DA analysis, the synthetic urine was spiked with 3 different concentrations of DA (5.0, 20.0, and $40.0 \text{ }\mu\text{mol L}^{-1}$), which were within the linear working range.

Synthetic saliva was prepared following the literature with adaptations [39] and was composed of a mixture of 0.7 g L^{-1} sodium chloride (99 % w/w), 1.2 g L^{-1} potassium chloride ($\geq 99 \text{ \% w/w}$), 0.26 g L^{-1} sodium phosphate dibasic (99% w/w), 0.33 g L^{-1} potassium thiocyanate, and 1.3 g L^{-1} urea (99 % w/w), solubilized in water. For SARS-CoV-2 analysis, the synthetic saliva was spiked with 4 different concentrations of (S1) protein (5.0, 10.0, 30.0, and 50.0 nmol L^{-1}), which were within the linear working range.

2.2. Manufacture of composite filament and Gpt-PLA electrodes

The PLA used to manufacture the composite filaments was obtained *in natura* as pellets, from 3DLAB (Minas Gerais, Brazil) and the graphite powder was obtained from Fisher Chemical™ (Hampton, EUA). Graphite-PLA (Gpt-PLA) filaments were easily fabricated after the solubilization of the matrix (PLA), and incorporation of graphite powder. Firstly, graphite powder (in varied composition, from 1 to 60% wt) was dispersed in 200 mL of a mixture of acetone and chloroform (3:1 v/v), for solubilization of the thermoplastic material, as reported in the literature [40], under magnetic stirring and heating to temperatures up to 70 °C during 30 min. Though the use of chloroform still provides a toxicity degree to the manufacturing process, its proportion is decreased, reducing the risk degree. A reflux system was employed (Fig. 1A) for avoiding the escape of solvents, and commercial vegetal oil, purchased from local stores, was used in the heating bath. An appropriate amount of PLA (totalizing 30 g of PLA and graphite) was added to the mixture and kept under constant stirring and heating for 3 h. The heating improved the incorporation of the graphite into the PLA matrix since guaranteed the dissolution of the polymer. After that, the obtained homogeneous mixture was immediately recrystallized by transferring all the content into a recipient containing 800 mL ethanol (Fig. 1B), and a uniform Gpt-PLA composite was obtained. The composite was filtered, being washed with ethanol as shown in Fig. 1C, and left to dry at 50 °C, overnight (Fig. 1D).

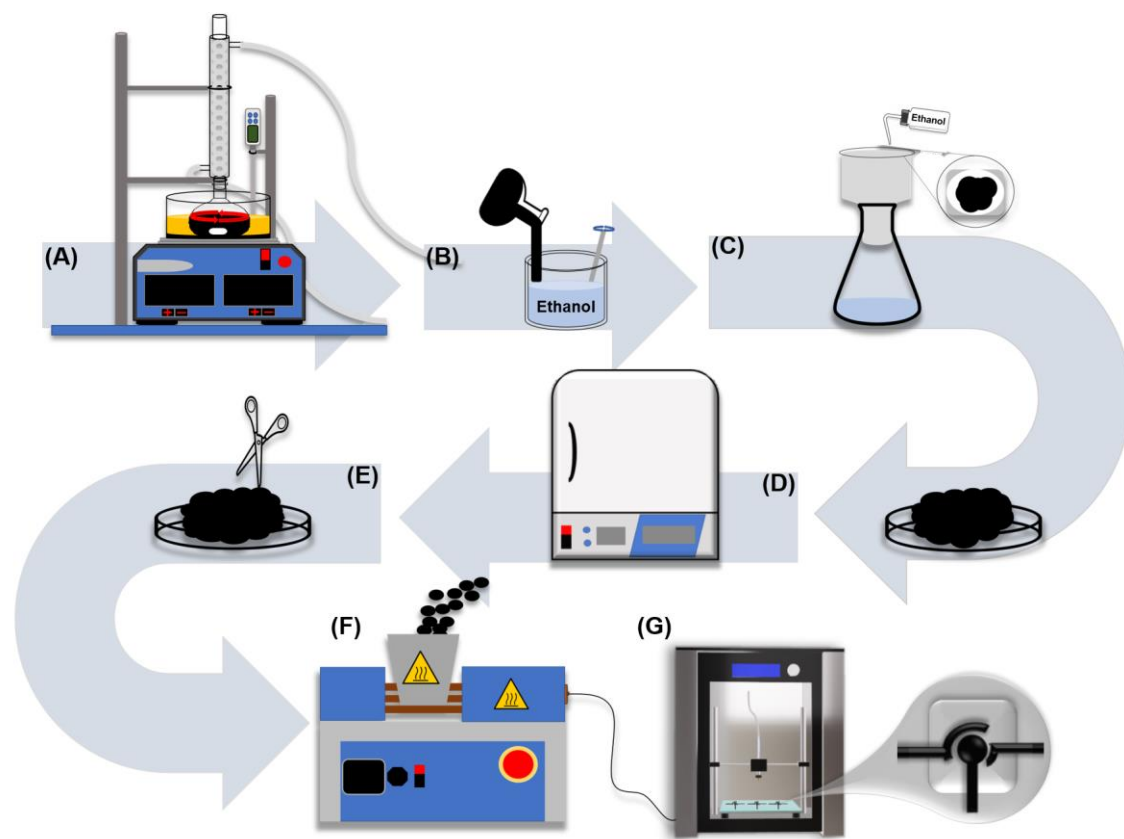


Figure 1. Representative scheme for the production of the improved Gpt-PLA conductive filaments. (A) incorporation of graphite powder on PLA and a reflux system under constant stirring and heating; (B) recrystallization of the composite (Gpt-PLA) in ethanol; (C) filtration of the composite constantly washing with ethanol; (D) drying step on the oven at 50 °C; (E) cut into small parts; (F) composite extrusion step and (G) 3D printing of the electrochemical sensor.

The filaments were then obtained after the cutting of the composite in small pieces (< 2 cm), with the aid of a scissor, previously cleaned with ethanol (Fig. 1E), and the pieces were subsequently placed into the Filmaq3D[®] extruder (Fig. 1F), which was operated at a temperature of 200 °C. The obtained filaments were used for 3D printing the electrodes (counter, reference, and working electrodes), originally designed as presented in Fig. 1G, using appropriate software (Blender[®]), and a non-conductive base

was also printed using PLA for the coupling of the electrodes (Fig. 1G), forming a three-electrode system. The electrochemical cell was then composed of the three-electrodes system, where an aliquot of solution (150 μL) was placed on the surface of the electrodes, closing the electrochemical system. All analyses were performed after simple mechanical polishing of the electrodes, using humid sandpaper obtained from local stores, until to obtain smooth surfaces. For better comprehension of the whole process, a time-lapsed video showing the manufacturing process of the filaments, as well as the 3D printing of the electrodes and assembling of the electrochemical cell is available. Also, the STL files for 3D printing are available on the journal website.

For comparison of the results, the commercial filaments based on graphene (Black Magic[®], acquired from Black Magic 3D - New York, USA), and carbon black (Proto Pasta[®], obtained from Proto Pasta, Vancouver, USA) were used for 3D printing of the electrodes by FDM, and the electrochemical cells and platforms were printed using non-conductive PLA thermoplastic filament, from Sethi3D (Campinas, Brazil).

2.3. Biosensor fabrication

For the diagnosis of COVID-19, a recombinant SARS-CoV-2 spike (S1) protein was used as antigen and a SARS-CoV-2 spike antibody (S1 Ab) from Sino Biological (Wayne, USA) were used. To prepare the immunosensor, initially, the antibodies were covalently bonded to the electrode surface, using 20 μL of a solution containing 10.0 mmol L^{-1} EDC and 20.0 mmol L^{-1} NHS in PBS 1x (pH = 7.4), dropped directly at the electrode surface and rested for 1 h, followed by 1 h immobilization of 1 $\mu\text{g mL}^{-1}$ antibody solution (20 μL) in PBS 1x (pH = 7.4). The subsequent drop-casting of 20 μL BSA solution (1% w/v) in PBS 1x (pH = 7.4) was performed and incubated for 30 min

to block any interaction sites available in the Gpt-PLA. Fig. 2 presents a representative scheme of the steps involved in the fabrication of the immunosensor.

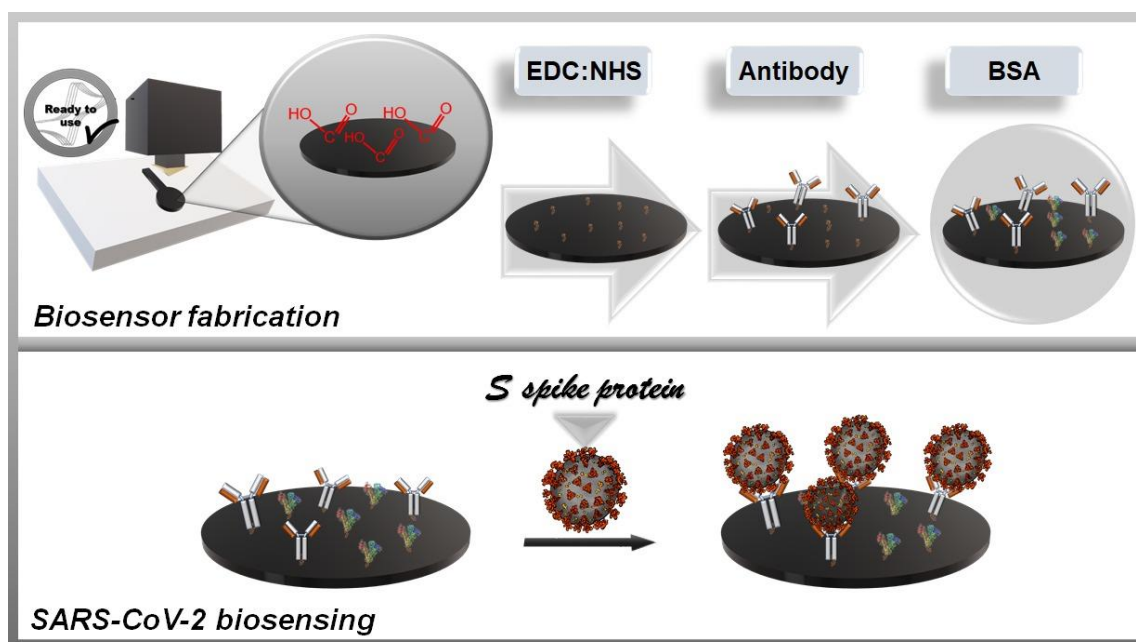


Figure 2. Representative scheme of the involved steps in the fabrication of the immunosensor.

The electrode was rinsed after each step with PBS 1x and dried in air. After that, the immunosensor was ready for the detection of the virus spike protein. The detection was performed upon 30 min incubation of different concentrations of antigen diluted in PBS 1x (pH = 7.4). All experiments were performed at room temperature (25 °C).

2.4. Instrumental and apparatus

A Sethi3D S3 3D printer (Campinas, Brazil) was used for printing the structures and electrodes used in this work, controlled by the software Simplify 3D™, for the manufacturing of the structures by the FDM technique. A Filmaq3D® extruder (Curitiba, Brazil) was used for the extrusion of the obtained composites.

All electrochemical measurements were performed on a potentiostat/galvanostat PGSTAT204 Metrohm (Eco Chemie) guided by the NOVA software (version 1.11), which was also used for data acquisition and treatment. Background-correction was used for voltammetric detection of UA and DA for better viewing of the peaks, the treatment was performed using the “moving average” algorithm, with window size set to 2, available in the NOVA software (version 1.11).

For the characterization of the materials, thermogravimetric analysis (TGA) was performed using a TGA 55 from TA INSTRUMENTS, in a gradual temperature increase of 10 °C per minute, varying from 25 to 1000°C under oxidizing atmosphere. The Raman spectra were obtained in a LabRam HR Evolution Spectrophotometer (HORIBA), using a 532 nm laser at 50 mW power over the range of 4000 to 100 cm⁻¹. Fourier-transform infrared spectroscopic (FTIR) analysis was performed using a Tensor II (Bruker) spectrophotometer. Scanning electron microscopy (SEM) from Thermo Fisher Scientific model Prisma E with ColorSEM Technology and integrated energy-dispersive X-ray spectroscopy was used for the acquirement of SEM images. Contact angle images were obtained by a drop-casting of deionized water in the electrochemical cell, involving all three electrodes surface. The contact angle images were obtained using a lab-made apparatus by launching a drop of deionized water into the electrochemical cell, involving the surface of the three electrodes. After 10 s of drop insertion, the images were obtained, and the angle between the tangent drawn at the liquid phase (water droplet) and the substrate surface was measured (n = 3), using an apparatus previously described in the literature [41].

For initial studies, a conventional cylindrical 3D printed electrochemical cell, similar to the developed by Cardoso et al. [18], was used for the electrochemical measurements. The 3D printed cell was manufactured using acrylonitrile butadiene

styrene (ABS) filament, and consisted of a cylindric container, with a cover containing holes for the coupling of the conventional counter (Pt wire) and reference ($\text{Ag}|\text{AgCl}|\text{KCl}_{(\text{sat.})}$) electrodes. The base of the cylinder presented a hole for positioning the working electrode (3D printed plate), over a stainless-steel plate for electrical contact, and under a rubber O-ring for defining the electrode area as 0.18 cm^2 and avoiding leaking of solutions. The bottom support and screws were 3D printed in ABS and were used to assemble the cell. Electrochemical assays were performed using the cell design presented in Fig. 1G, using a single drop of $150 \mu\text{L}$ of solutions. Gpt-PLA was used as reference and counter electrodes, and Gpt-PLA, or commercial (Black magic[®] (G-PLA) and/or Proto pasta[®] (CB-PLA)) as working electrodes. The working electrode (circular-like structure) presented a diameter of 4 mm (geometric area of 0.13 cm^2).

3. Results and discussion

Firstly, the filaments were produced through the incorporation of different amounts of graphite (1, 15, 25, 30, 35, 40, 50, 55, 60% wt.). TGA analysis was performed to understand the thermal stability and the printability of the designed filaments, and also to validate the incorporation of graphite percentage mass in the PLA matrices (Fig. 3A). As can be seen in TGA data for the raw polymer, a weight loss for PLA occurs at around $300 \text{ }^\circ\text{C}$ and corresponds to the decomposition of PLA to carbon dioxide, carbon monoxide, and further cyclic oligomers up to the monomer unit [42,43]. After the addition of conductive fillers, the filaments presented a slight improvement in thermal stability. According to the literature, the presence of conductive material in the polymeric matrix increases the heat conduction, consequently, it inhibits the emission of decomposition production during the degradation [42,44]. The filament containing

graphite did not decompose before 250 °C, which indicated that a printing temperature of 200 °C is appropriate for 3D printing the electrodes.

Moreover, a conventional electrochemical cell was employed to evaluate and choose an optimized conductive filament regarding the %wt. of graphite and the respective electrochemical response. For this, cyclic voltammograms were performed using a 3D printed plate as a working electrode, a Pt wire as the counter electrode, and Ag|AgCl|KCl_(sat.) as the reference electrode, and employing a 1.0 mmol L⁻¹ [Fe(CN)₆]^{3-/4-} electrochemical probe in 0.1 mol L⁻¹ KCl. The cyclic voltammograms were performed for filaments with compositions between 30 and 50% wt. of graphite (Fig. S1), lower amounts of graphite presented a non-conductive behavior, while a material with more than 50% presented very low printability. It is noteworthy to mention that, though 50% wt. graphite presented better reversibility (lower ΔE_p, corresponding to 136 mV), as well as improved current response, this composite was not chosen due to printing difficulties and the obtention of a highly brittle structure. The filament containing 40% wt. graphite also provided a satisfactory current response, though the reversibility of the process was negatively affected (higher ΔE_p, corresponding to 264 mV), being possible to observe a slower electron transfer kinetic. In this sense, it can be observed that the higher amount of PLA, decreasing the electron transfer kinetic, providing CVs with higher peak-to-peak separation. The filament with better characteristics (high printability coupled with good electrochemical response) contained 40% wt. of graphite on the PLA. Therefore, this filament was used for printing all the electrodes, and the physicochemical characterizations were performed for this material.

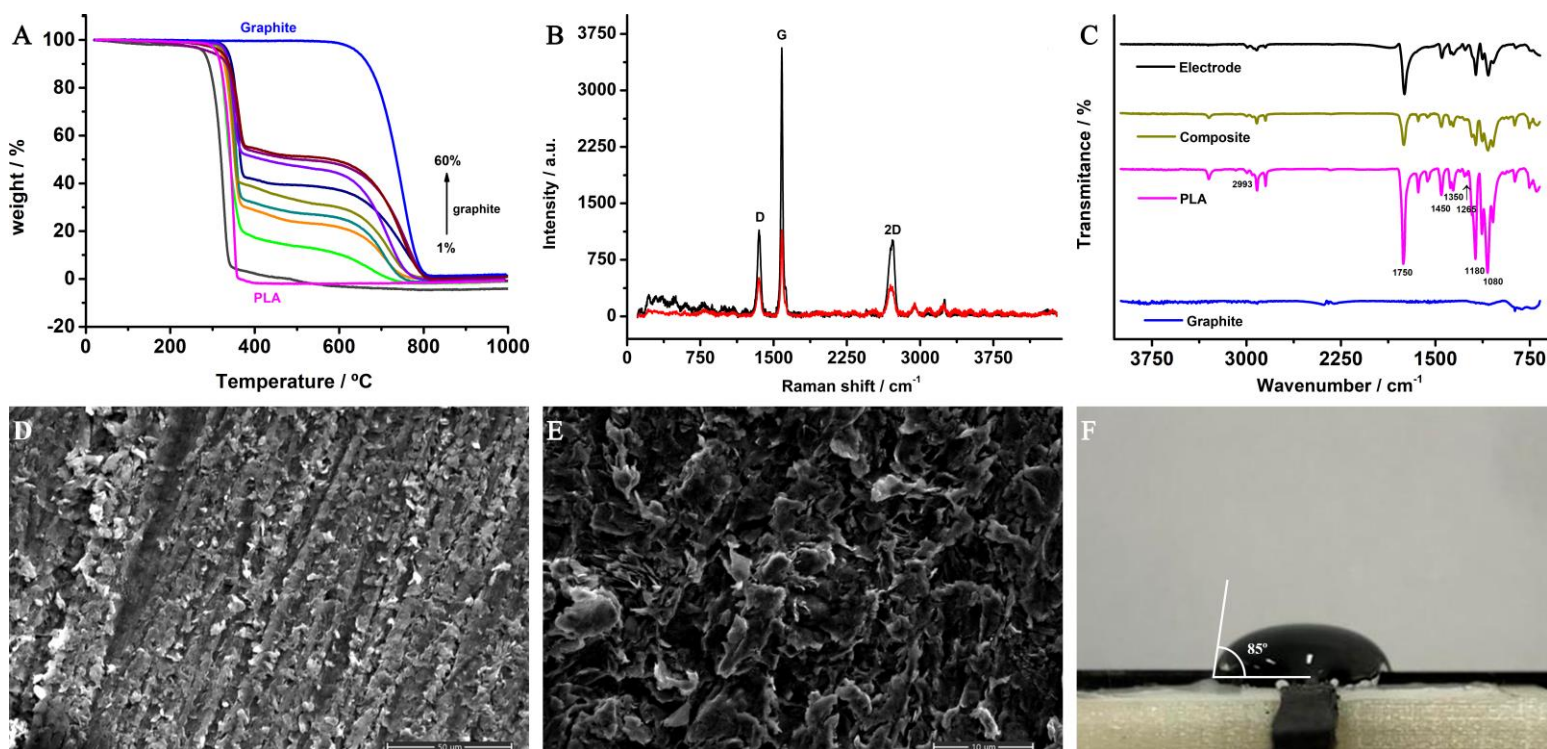


Figure 3. Physicochemical characterizations: A) Thermogravimetric analysis for raw PLA, graphite powder, and GP-PLA filaments containing 1, 15, 25, 30, 35, 40, 50, 55, 60 %wt. graphite; B) Raman spectra for Gpt-PLA (40% wt.) filament (red line) and 3D printed electrode (black line); C) FTIR spectra for raw PLA, graphite powder, Gpt-PLA (40% wt.) filament and 3D printed electrode; D) and E) SEM analysis of 40% wt. Gpt-PLA 3D printed electrode after 2000 and 8000 amplification factors, respectively, and F) Contact angle image.

The Raman spectra of the filament and the 3D printed electrode are presented in Fig. 3B. The most prominent features in the Raman spectra for all graphitic materials are the presence of the D (1350 cm^{-1}), G (1585 cm^{-1}), and 2D (2715 cm^{-1}) vibrational bands. The G band in the Raman spectra is related to the presence of in-plane stretching vibration of the sp^2 carbon atoms [45,46]. The D and G vibrational bands indicate the presence of defects, such as sp^3 and sp carbon networks, vacancies, edges sites, and

heteroatoms. The 2D signal is associated with the D and G band combination mode in graphitic materials [45,47]. It can be observed from Fig. 3B that the 3D printed electrode provided higher intensity bands than the filament. This can be attributed to the fact that the electrode was previously polished, and, therefore, the graphite particles are more exposed in comparison to the filament.

FTIR spectra were obtained for the analysis of the surface composition of the materials used for the synthesis of the composite (PLA and graphite), and for the obtained composite and electrodes (to observe changes after the extrusion and 3D printing processes). The obtained FTIR spectra are presented in Fig. 3C, which these results show the characteristic fingerprint of PLA, with peaks related to carboxylic and carbonylic groups, and C-H, C=C, and C-O-C bonds. Peaks observed between 2800 to 3000 cm^{-1} refer to aliphatic structures (C-H compounds) present in the PLA [6,48]. The peaks between 1000 and 1800 cm^{-1} are characteristic of oxygenated compounds. The vibration of the carboxyl and/or carbonyl groups of the PLA is detected at 1732 and 1450 cm^{-1} [6,48]. A very low intense peak at 1580 cm^{-1} referring to the vibrations of the C=C group due to the sp^2 hybridization of the graphite is observed [49]. Peaks at 1180 and 1080 cm^{-1} are attributed to the PLA C-O-C elongation vibration [6,48,50]. As can be seen, the peaks from PLA material are observed in the composite and electrode structures, however, with very lower intensity, since only 60% of the final material is PLA. The presence of carboxylic groups at the electrode surface, observed by FTIR analysis, enabled the construction of the immunosensor with no need for further electrode modification with gold nanoparticles, as frequently reported in the literature [32,51,52].

SEM images of the Gpt-PLA electrode were recorded after two amplification factors (2000 and 8000), as can be seen in Fig. 3D and E, respectively. It is possible to

observe the graphite sheets well distributed through the composite structure (Fig. 3D) after higher amplification (Fig. 3E). Irregularly shaped graphite sheets and many sharp edges can be observed, providing a non-uniform surface as expected for thermoplastic composites [23,53], which can provide active sites capable of improving the interaction of the species with the surface.

The contact angle was measured for the 3D printed electrode surfaces, this parameter gives information regarding the hydrophilicity behavior of a surface. It is known that graphitic materials present hydrophobic characteristics [54], however, due to the presence of oxygenated groups from the matrix of the composite filament (PLA), confirmed by FTIR analysis, PLA contributes to a more hydrophilic surface. Since the composite presents a slightly higher amount of PLA, the material provided a contact angle tending more to a hydrophilic behavior ($85^{\circ} \pm 1.2^{\circ}$), however, a limit for hydrophobicity, as expected.

Cyclic voltammograms were recorded for Gpt-PLA working electrodes in a conventional cell to evaluate the performance of the obtained composite filaments, using the $1.0 \text{ mmol L}^{-1} [\text{Fe}(\text{CN})_6]^{3-/4-}$ electrochemical probe in $0.1 \text{ mol L}^{-1} \text{ KCl}$. For a better comprehension of the obtained results, working electrodes were also 3D printed using commercial filaments. In these tests, the electrodes were not submitted to any surface treatment, only surface polishing for obtaining a smooth surface (removing the lines prevenient of the printing process), and the cyclic voltammograms obtained are shown in Fig. 4A.

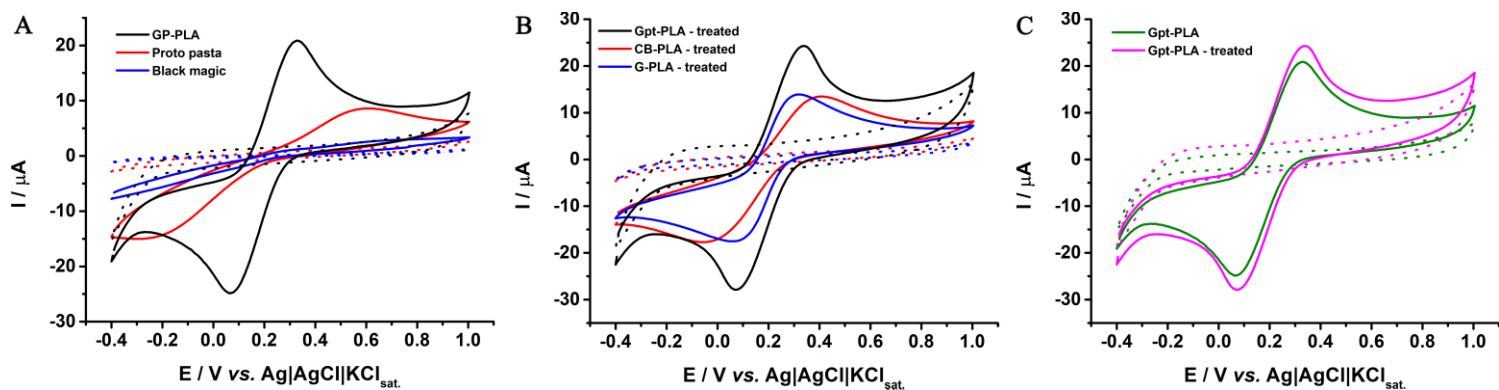


Figure 4. Cyclic voltammograms for 1.0 mmol L⁻¹ [Fe(CN)₆]^{3-/4-} in 0.1 mol L⁻¹ KCl in **A)** Gpt-PLA, CB-PLA, and G-PLA after polishing in sandpaper; **B)** Gpt-PLA, CB-PLA, and G-PLA after electrochemical pre-treatment and; **C)** Gpt-PLA before and after electrochemical treatment. Scan rate: 50 mV s⁻¹.

As can be seen in Fig. 4A, the Gpt-PLA electrode, without treatment, provided a better electrochemical response when compared to graphene (G-PLA) and carbon black (CB-PLA) commercial filaments. The electrochemical characteristics obtained from Fig. 4 are summarized in Table 1. A higher current response was observed, with a current ratio (I_{pa}/I_{pc}) closer to unity (1.05), indicating better reversibility of the process on this surface, when compared to G- and CB-PLA electrodes. Moreover, the peak-to-peak separation (ΔE_p) on Gpt-PLA was smaller, confirming the better reversibility of the process.

This result was already expected for commercial filaments, once it has been shown in the literature that those surfaces require a surface pre-treatment for removing the excess of non-conductive PLA from electrode surfaces [16,19,55] (only around 8% of the filaments is composed of conductive materials) [3]. This result allows us to conclude that the use of higher concentrations of conductive material in the

manufactured filament can be related to the improvement of the performance of the 3D printed Gpt-PLA electrode without pre-treatment since in this case, it is observed the presence of smaller amounts of polymers, which can “block ” the active sites of carbon, what provides slower electron transfer kinetics [56].

To also examine the effect of surface activation on the performance of 3D printed Gpt-PLA electrodes, electrochemical pretreatments were carried out with all materials under evaluation (Gpt-, G- and CB-PLA). An electrochemical pretreatment based on the application of +1.4 V for 200 s, followed by the application of -1.0 V for 200 s, in presence of 0.5 mol L⁻¹ NaOH, very employed in the literature for electrodes produced from commercial filaments [57,58], was explored. Fig. 4B presents the cyclic voltammograms for 1.0 mmol L⁻¹ [Fe(CN)₆]^{3-/4-} on electrochemically treated Gpt-, G- and CB-PLA electrodes. A significant improvement of electrochemical responses was observed for G- and CB-PLA electrodes, including higher peak currents, lower I_{pa}/I_{pc} ratio, and lower ΔE_p (Table 1), indicating the better reversibility of the redox process on these surfaces after treatment. Still, Gpt-PLA presented superior responses, even when compared to the response obtained with the non-treated Gpt-PLA electrode. The surface treatment did not provide a significant increase in the analytical response of Gpt-PLA (Fig. 4C), with no significant variation in the peak current and potential separation, which probably occurred because the amount of PLA on the electrode is lower when compared to the others. Therefore, the new sensor obtained from the proposed conductive filament proved to be effective and no surface treatment is necessary for the obtainment of satisfactory electrochemical responses. A probable hypothesis for Gpt-PLA not requiring activation is that it presents a high amount of conductive material in its matrix (40% wt.), which corresponds to approximately 5 times more than commercial filaments. In this sense, a simple polishing step of the electrode surface to

remove the excess of PLA is enough to employ this material as an electrochemical sensor. Due to the lower amount of polymer on the electrode surface, the effects on the activation with NaOH are not so evident. As can be observed in Fig. S2, higher concentrations of PLA on the electrode provide a better improvement on the electrochemical response of $[\text{Fe}(\text{CN})_6]^{3-/4-}$ after NaOH activation. Thus, the greater amount of PLA on the electrode, the more effective is the NaOH treatment.

Table 1. Electrochemical characteristics for 3D printed sensors in presence of 1.0 mmol L^{-1} $[\text{Fe}(\text{CN})_6]^{3-/4-}$ obtained from cyclic voltammetric experiments.

Conductive filament	$I_{pa} / \mu\text{A}$	$I_{pc} / \mu\text{A}$	I_{pa} / I_{pc}	$\Delta E_p / \text{mV}$
G-PLA	0.54	-0.17	3.18	869
G-PLA treated*	15.10	-13.50	1.12	260
CB-PLA	5.67	-4.18	1.36	904
CB-PLA treated*	12.20	-11.00	1.11	466
Gpt-PLA	19.80	-18.90	1.05	264
Gpt-PLA treated*	20.50	-20.60	0.995	267

* Electrochemical pre-treatment: application of +1.4 V for 200 s, followed by the application of -1.0 V for 200 s, in presence of 0.5 mol L^{-1} NaOH.

As the CV response strongly depends on the electroactive probe employed, the use of a different redox probe was also evaluated. Cyclic voltammograms were recorded at 50 mV s^{-1} for the electrochemical redox probe $[\text{Ru}(\text{NH}_3)_6]^{3+/2+}$ in 0.1 mol L^{-1} KCl and, Fig. S3 presents the obtained results. As can be seen in Fig. S3-A, the electrochemical behavior obtained using commercial filaments CB- and G-PLA without surface treatment is superior to the observed using $[\text{Fe}(\text{CN})_6]^{3-/4-}$, with well-defined oxidation and reduction peaks and lower ΔE_p , showing better reversibility of the processes. This response is in agreement with the reported in the literature, which shows that the use of CB-PLA presents a nearly ideal electrochemical behavior for ruthenium(III)

acetylacetonate redox probe, even for non-activated electrodes probe [9], with ΔE_p values ranging from 85 to 95 mV at scan rates of 25 mV s⁻¹. A higher ΔE_p value was found in the present work for CB-PLA, however, the CVs were performed employing 50 mV s⁻¹. Besides, the difference in ΔE_p can also be attributed to the 3D printed pseudo-reference electrode (Gpt-PLA) employed in this work, in comparison to the freshly annealed gold wire which served as a quasi reference from the literature [9]. In addition, literature shows that the use of ruthenium(III) acetylacetonate as a redox probe provides improved electrochemical behavior even when a different carbon loading, such as carbon nanotubes (CNTs) is employed. In this regard, Escobar et al. [12] have employed a CNT-PLA 3D printed electrode, obtaining a peak-to-peak separation of 80 mV, while Vaněčková and collaborators [14] have observed ΔE_p values between 80 and 95 mV for treated and non-treated surfaces.

When comparing CB- and G-PLA to Gpt-PLA, a superior current response is observed for the last, though a slightly higher ΔE_p is observed (236 mV, when compared to 222 and 161 mV for G-PLA and CB-PLA, respectively). After being submitted to the electrochemical surface treatment, the performance of CB- and G-PLA electrodes was significantly improved (Fig. S3-B). A significant decrease in ΔE_p is observed for G-PLA and CB-PLA, reaching 153 and 116 mV, respectively. In addition, a considerable increase in the peak current for G-PLA can be observed, however, the peak current obtained in this surface is comparable to Gpt-PLA without surface treatment, confirming that the performance of Gpt-PLA is adequate for different redox probes, without being submitted to surface treatments.

Electrochemical characterization was performed for evaluation of Gpt-PLA facing G- and CB-PLA electrodes, using the developed three-electrode cell and the

redox probe ferrocenemethanol (FcMeOH) since better-defined peaks were observed, especially for untreated G- and CB-PLA.

A study using cyclic voltammetry was performed in a range from 0.01 to 0.1 V s⁻¹ in presence of 1.0 mmol L⁻¹ FcMeOH for untreated (Fig. S4-A) and treated (Fig. S4-B) G-PLA, and untreated (Fig. S4-C) and treated (Fig. S4-D) CB-PLA, as well as untreated Gpt-PLA (Fig. S4-E), and the respective plots of anodic and cathodic peak currents as a function of the square root of the scan rate. A linear behavior was observed for all surfaces (except untreated G-PLA, which was not following a tendency, probably due to the poor exposition of graphene on the electrode surface for the presence of polymeric material which can “block” the active sites of carbon, thus providing a slower electron transfer kinetics), indicating a mass transport process controlled by the diffusion of FcMeOH species on the electrode surfaces. The electrochemically active surface area of the electrodes was obtained using the Randles-Ševčík equation, and the diffusion coefficient for FcMeOH was 7.6 x10⁻⁶ cm² s⁻¹, previously reported in the literature [59,60].

The obtained values are presented in Table 2, as well as the relative electrochemically active surface area values in percentage, considering the geometric area of the electrodes. It can be seen that the G- and CB-PLA electrodes, presented a similar electrochemically active surface area after the pre-treatment, where about 82% of the electrode surface was electrochemically active, while Gpt-PLA provided a higher electrochemically active surface area than both, corresponding to an increase in the electroactive area of 62%.

Additionally, the heterogeneous electron transfer rate (HET) constant k_{obs}^0 was determined by the Nicholson method [61] for the studied surfaces using the FcMeOH redox probe and CV data by the Equation 1 :

$$\psi = k^0 [\pi D n \nu F / (RT)]^{-1/2} \quad \text{Equation 1}$$

Where ψ is a kinetic parameter, D is the diffusion coefficient for FcMeOH ($7.6 \times 10^{-6} \text{ cm}^2 \text{ s}^{-1}$), n is the number of electrons involved in the process, F is the Faraday constant, R the gas constant, and T the temperature (298 K). The function $\psi(\Delta E_p)$, is given by $\psi = (-0.6288 + 0.0021 \times \Delta E_p) / (1 - 0.017 \times \Delta E_p)$. ΔE_p is used to determine ψ from the experimentally recorded voltammograms. From this, a plot of ψ against $[\pi D n \nu F / (RT)]^{-1/2}$ allows k^0 to be determined.

In addition, k^0_{obs} was also obtained using electrochemical impedance spectroscopy (EIS) data from R_{ct} values [62] for the studied surfaces using the FcMeOH redox probe, employing Equation 2:

$$R_{\text{ct}} = \frac{RT}{F^2 k^0 C} \quad \text{Equation 2}$$

Where R_{ct} is the resistance to charge transfer, obtained by EIS data, R is the gas constant, T the temperature, F is the Faraday constant and C is the concentration of the electroactive species (1.0 mmol L^{-1}). The obtained k^0_{obs} values are presented in Table 2.

Higher k^0_{obs} value was observed for the proposed Gpt-PLA electrode (without surface treatment) using both methods, indicating faster HET kinetics compared to G- and CB-PLA electrodes (with surface treatment), which resulted in improved cyclic voltammograms obtained in this surface [63]. Though k^0_{obs} values obtained from CV and EIS should theoretically present the same values, here it can be observed a considerable reduction in k^0_{obs} values from EIS to CV determined values (up to 49% decrease). This can be attributed to the polymeric matrices of the electrodes since the currents are being affected by the presence of the polymers capable of “blocking” the carbon active sites, thus providing a slower electron transfer kinetics [56].

Table 2. Parameters obtained from the electrochemical characterization with the proposed and commercial filaments.

Conductive filament	$k_{\text{obs}}^0 \times 10^{-6} /$ cm s^{-1}		$\Delta E_p /$ V	R_{ct} / Ω	Electrochemically active surface area /	
	CV	EIS			mm^2	%
G-PLA treated*	6.1	10.1	0.196	26.4	10.26±0.07	81.6±0.5
CB-PLA treated*	5.0	9.1	0.166	29.4	10.26±0.06	81.6±0.5
Untreated Gpt-PLA	7.5	14.6	0.173	18.2	16.72±0.03	133.0±0.2

* Electrochemical pre-treatment: application of +1.4 V for 200 s, followed by the application of -1.0 V for 200 s, in presence of 0.5 mol L⁻¹ NaOH.

Finally, EIS was employed to evaluate the charge transfer resistance (R_{ct}). The Nyquist plots obtained for untreated Gpt-PLA, and the commercial treated G-PLA and CB-PLA are shown in Fig. S5. The R_{ct} obtained values for the sensors are presented in Table 2. From the R_{ct} values, it can be inferred that the untreated Gpt-PLA electrode showed lower resistance to charge transfer, thus, the electron transfer is favored in this surface, in agreement with the k_{obs}^0 value obtained. Also, the treated G-PLA electrode provided a surface with slightly lower R_{ct} than the treated CB-PLA electrode, as well as higher k_{obs}^0 indicating that the redox process is favored using the treated G-PLA electrode when both G-PLA and CB-PLA electrodes present the same electrochemically active surface area after electrochemically treated.

Thus, electrochemical characterization showed the superior performance of the electrodes fabricated using the manufactured composite filament, with higher electrochemically active surface area observed, satisfactory reversibility for the studied redox probes, faster HET, and lower R_{ct} values when compared with commercial filaments, with the advantage of being a ready-to-use filament (no pre-treatment step is

necessary), additionally to be a lab-made material, of simple fabrication and relatively low-cost. The applicability of the proposed material was evaluated towards the determination of uric acid in synthetic urine samples using voltammetric techniques.

3.1. Voltammetric determination of biomarkers

Uric acid is a relevant species in biological fluids. It is an oxidative-stress non-enzymatic defense molecule in the human body [64]. In addition, abnormal blood levels of UA can indicate some renal pathophysiology [65]. For this reason, the determination of UA was selected as a proof-of-concept.

Fig. 5 shows the cyclic voltammetric response for 1.0 mmol L^{-1} UA in BR buffer solution (pH 2.0) using the untreated Gpt-PLA electrode, and, for comparison, the results obtained with untreated and treated G-PLA and CB-PLA electrodes are also shown. As can be seen in Fig. 5, the cyclic voltammetry on the “as printed” G- and CB-PLA displayed ill-defined waves for UA. These results are in agreement with recent studies in the literature that showed the need for the activation procedure of 3D printed sensors to remove the insulating PLA matrix [7,15,17,19,25]. When the 3D printed electrodes using commercial filaments (G- and CB-PLA) were subjected to an electrochemical treatment according to reported in the literature [15], a significant improvement response was achieved. After the treatment, a twice higher peak current was obtained for the CB-PLA electrode and impressive improvement for the G-PLA electrode (the ill-defined peak before surface treatment) was observed.

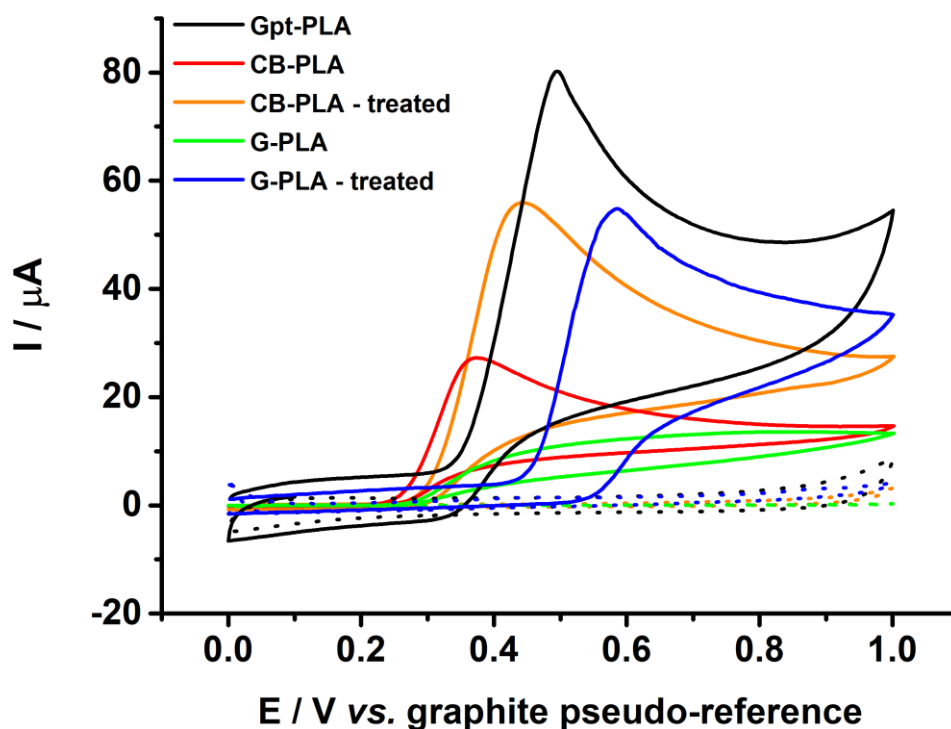


Figure 5. Cyclic voltammograms for 1.0 mmol L⁻¹ UA in 0.1 mol L⁻¹ BR buffer (pH 2.0) on 3D printed Gpt-PLA and G-PLA and CB-PLA before and after electrochemical pre-treatment. Scan rate: 50 mV s⁻¹.

Moreover, Fig. 5 has shown a well-defined peak for UA at around +0.5 V (vs. graphite) and superior performance (1.4 times higher current response) of the produced composite filament (Gpt-PLA) without treatment in comparison of G-PLA and CB-PLA filaments after electrochemical surface treatment. Therefore, the Gpt-PLA sensor is very promisor for the electrochemical oxidation of UA.

Next, the 3D printed Gpt-PLA electrode was employed for the quantification of UA using differential pulse voltammetry (DPV). The DPV parameters were systematically optimized (univariate tests), using a solution containing 30.0 μmol L⁻¹ UA in 0.1 mol L⁻¹ BR buffer (pH 2.0) as the supporting electrolyte. Fig. S6-A, S6-B, and S6-C showed the DPV signals obtained in the optimization studies for modulation amplitude, modulation time, and step potential, respectively. The evaluated ranges and

respective optimized values are given in Table S1. According to these results, the best condition for UA determination by DPV was achieved using a step potential of 5 mV, modulation amplitude of 80 mV, and a modulation time of 30 ms.

Using the selected DPV conditions for UA detection, a wide linear range from 0.5 to 150.0 $\mu\text{mol L}^{-1}$ ($R^2 = 0.998$) was obtained, as shown in Fig. 6. From this calibration curve, the values of the limit of detection (LOD) and quantification (LOQ) obtained were 0.07 and 0.23 $\mu\text{mol L}^{-1}$, respectively, with the sensibility of 0.05 $\mu\text{A } \mu\text{mol}^{-1} \text{ L}$. Table 3 summarizes the analytical parameters obtained from the data shown in Fig. 6. The limits of detection (LOD) and quantification (LOQ) were calculated based on the IUPAC definition ($\text{LOD} = 3.3\sigma/s$ and $\text{LOQ} = 10\sigma/s$), where σ is the standard deviation of baseline noise and s is the analytical sensitivity of the calibration curve.

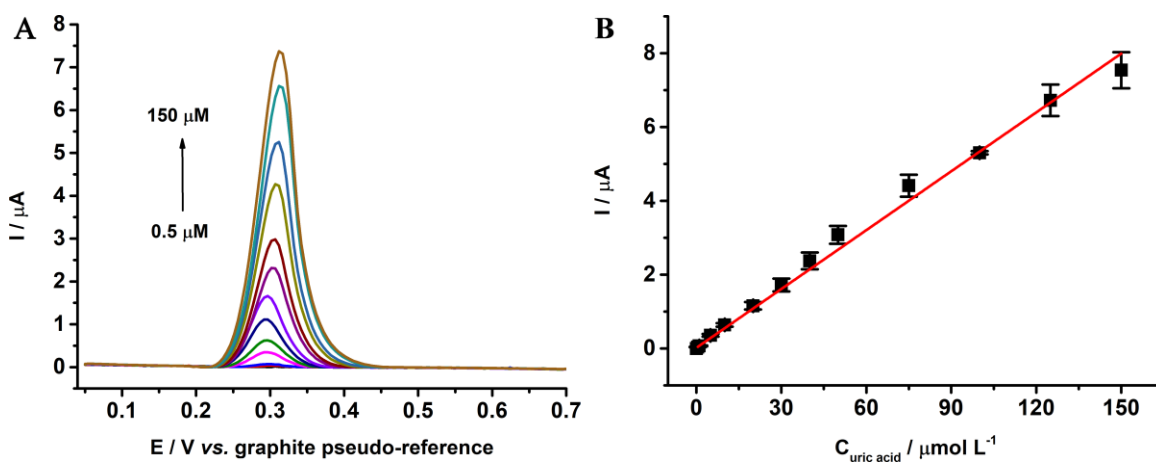


Figure 6. Differential pulse voltammograms for increasing concentrations of UA (0.5, 1.0, 5.0, 10.0, 20.0, 30.0, 40.0, 50.0, 75.0, 100.0, 125.0 and 150.0 $\mu\text{mol L}^{-1}$) in 0.1 mol L^{-1} BR buffer (pH 2.0). DPV parameters: 80 mV (modulation amplitude); 30 ms (modulation time); 5 mV (step potential).

The inter-electrode precision was also evaluated based on the measurement of the current peak for different electrodes ($n = 5$) in the presence of $10.0 \mu\text{mol L}^{-1}$ UA (also shown in Table 3). The RSD values were $<12\%$ in which indicates high precision in the construction of the 3D printed Gpt-PLA sensor for UA determination. Also, the repeatability of the sensor was evaluated after 13 consecutive DPV recordings of $100.0 \mu\text{mol L}^{-1}$ UA (presented in Table 3), and an RSD $<5\%$ was obtained (Table 3).

Table 3. Analytical features for the detection of UA using Gpt-PLA 3D printed electrode.

Characteristics	Values
Linear range / $\mu\text{mol L}^{-1}$	0.5 to 150.0
R^2	0.998
Sensitivity / $\mu\text{A } \mu\text{mol}^{-1} \text{L}$	0.05
LOQ / $\mu\text{mol L}^{-1}$	0.23
LOD / $\mu\text{mol L}^{-1}$	0.07
Intra-electrode (RSD, $n = 13$)	4.8
Inter-electrode (RSD, $n = 5$)	12.0%

Ho, Ambrosi, and Pumera [66] displayed the construction of 3D metal printed electrode electrochemically modified with a gold layer for UA determination in an aqueous solution. Using the DPV technique, the authors showed a linear range between $0.1\text{-}1.0 \text{ mmol L}^{-1}$ with a LOD value of $84.0 \mu\text{mol L}^{-1}$. After that, Cardoso and coworkers showed the simultaneous determination of UA and nitrite in biological fluids samples using 3D printed graphene-PLA electrodes [25]. The authors highlighted that the electrochemical response of UA was relatively poor in the non-treated 3D printed electrode because of the high amount of non-conductive PLA. Therefore, for the

construction of the sensors, the 3D printed electrode was subjected to mechanical and immersion in DMF for treatment. After the activation, the authors obtained a good linear range from 10.0 to 70.0 $\mu\text{mol L}^{-1}$ and a LOD of 0.5 $\mu\text{mol L}^{-1}$, using the DPV technique.

Although the authors reached good results using the 3D printing technique for electrode construction in both works, activation or modification procedures of the electrode surface were required to obtain satisfactory results for UA detection. On the other hand, the homemade Gpt-PLA filament was found to be a promising material for the construction of a UA sensor without the need for treatment using toxic organic solvents or expensive procedures.

Moreover, UA can be found in a concentration range from 0.12 to 0.38 mmol L^{-1} in blood serum and this value should be lower than 4.50 mmol L^{-1} per day in urine [67,68]. Thus, the LOD (0.07 $\mu\text{mol L}^{-1}$) obtained for this new sensor is useful for the detection of UA in these types of samples.

As a proof of concept, a synthetic urine sample was analyzed by the standard addition method, in which the sample was 40 times diluted in the supporting electrolyte. The analysis was performed under optimized DPV conditions, and the diluted synthetic urine was then fortified with increasing concentrations of UA (10.0 to 40.0 $\mu\text{mol L}^{-1}$). The obtained voltammograms are presented in Fig. S7-A, and the respective standard addition curve can be seen in Fig. S7-B.

From Figure S7-B, the estimated UA concentration was 9.01 $\mu\text{mol L}^{-1}$, which corresponds to a satisfactory recovery value of 90.1% in synthetic urine. This result demonstrates the effectiveness of the sensor since the recovery presented a value close to the original. Furthermore, it is noteworthy that synthetic urine was prepared with different types of salts and organic compounds, which is free from interference,

demonstrating that there is no significant matrix effect for the analysis in the proposed sample.

As well as UA, the detection of DA is of great importance. DA is an important neurotransmitter in the mammalian central nervous system, capable of controlling cognitive functions and facilitating the communication between the brain neurons, directly related to neurological disorders, such as Parkinson's disease [69,70]. In this sense, and as a proof-of-concept, we also demonstrate the applicability of the developed sensor for the detection of this molecule.

The electrochemical behavior of DA was firstly evaluated by cyclic voltammetry. For this study, 1.0 mmol L⁻¹ DA was employed, using 0.1 mol L⁻¹ PBS (pH 7.0) as the supporting electrolyte and the untreated Gpt-PLA electrode. The obtained voltammogram, shown in Fig. S8, presents the well-defined redox peaks for DA, with an oxidation peak at approximately +0.38 V and a reduction peak in the reverse scan at approximately -0.07 V, providing a peak-to-peak separation of 450 mV, attesting that the manufactured Gpt-PLA responds to the presence of dopamine. Thus, the 3D printed Gpt-PLA electrode was employed for the quantification of DA using square wave voltammetry (SWV). The SWV operational parameters (step potential = 8 mV, modulation amplitude = 100 mV and frequency = 10 Hz) for DA detection in synthetic urine samples were selected from the literature [71]. Fig. S9 presents the obtained voltammograms for increasing concentrations of DA.

A linear behavior was observed for concentrations of DA ranging from 0.5 to 50 $\mu\text{mol L}^{-1}$ ($R^2 = 0.991$), with a LOD of 0.11 $\mu\text{mol L}^{-1}$ (IUPAC definition), and a sensitivity of 0.179 $\mu\text{A } \mu\text{mol}^{-1} \text{ L}$. As a proof-of-concept, a synthetic urine sample was analyzed, which was spiked with three known concentrations (5.0, 20.0, and 40.0 $\mu\text{mol L}^{-1}$) of DA. The concentrations of DA found for the fortified samples were 5.08 ± 0.21 ,

19.22 \pm 1.21, and 37.09 \pm 2.63 $\mu\text{mol L}^{-1}$, which correspond to recovery values from 92.7 to 101.6%, attesting the good performance of the 3D printed Gpt-PLA electrode.

The use of 3D-printed electrodes for the detection of DA was shown previously. In all articles, low LOD values for DA (1.67 $\mu\text{mol L}^{-1}$ [7], 0.24 $\mu\text{mol L}^{-1}$ [6], and 1.45 $\mu\text{mol L}^{-1}$ [72]) were only achieved after activation or pretreatment steps of the 3D printed working electrode. Here, a better result for DA detection (0.11 $\mu\text{mol L}^{-1}$) was obtained without the use of activation/pre-treatment steps (ready to use) of the Gpt-PLA 3D-printed sensor, saving analysis time and reagents.

Additionally, the synthetic urine studied presented UA in its composition in a concentration of 40.0 $\mu\text{mol L}^{-1}$ (considering the 10 times dilution), however, no interference signal was observed in DA detection. Once different techniques and supporting electrolytes, including different pH values were employed for UA and DA detection separately, the response of UA in SWV employing optimized parameters and conditions for DA detection provided a very low intense UA peak current, attesting that these conditions are not favoring UA oxidation process. Moreover, different oxidation potentials are required for DA and UA oxidation processes, which enabled the detection of DA without the interference of UA. The absence of interference was confirmed by the recovery values obtained for DA, attesting to the suitability of the method for DA detection in synthetic urine. Fig. S10 presents SWV voltammograms for the synthetic urine spiked with 3 different concentrations of DA in presence of UA.

The development of biosensors is also an alternative, after modifying the sensor with suitable probes, which can provide the development of rapid point-of-care tests to detect different types of pathogens. In this sense, next, we present the applicability of the fabricated filament as a 3D printed biosensor for the diagnosis of COVID-19.

3.2. Gpt-PLA immunosensor for SARS-CoV-2 determination

To show the versatility of Gpt-PLA, studies were performed for the development of an immunosensor for the diagnosis of COVID-19 based on the Gpt-PLA 3D-printed sensor. Cyclic voltammetry was used to evaluate the response of each immobilization step and the response of the final immunosensor for the virus spike protein was performed employing 1.0 mmol L^{-1} FcMeOH. As the surface of Gpt-PLA already provided enough functional attachments with available carboxylic groups as observed by FTIR analysis, the bonding of EDC-NHS was possible directly in the Gpt-PLA surface, thus eliminating previous steps for the immunosensor fabrication. The OH groups of the carboxylic acid were then covalently bonded to the double bonds present in the EDC-NHS, activating the surface COOH groups for a rapid covalent coupling to amino-functionalized biorecognition element [73,74]. Next, the S1 protein antibody, rich in carboxylic groups, was immobilized onto the electrode, releasing the intermediary NHS linker. The blockage of the electrode was performed with BSA solution (1% w/v), preventing nonspecific interactions [73]. After that, the immunosensor was ready-to-use, that is, with few steps of fabrication, a simple immunosensor was built.

Cyclic voltammetric measurements were obtained for 1.0 mmol L^{-1} of FcMeOH in 0.1 mol L^{-1} KCl, after each immunosensor fabrication step: Gpt-PLA, Gpt-PLA/EDC-NHS, Gpt-PLA/EDC-NHS/Ab, and Gpt-PLA/EDC-NHS/Ab/BSA, and after the addition of 50.0 nmol L^{-1} antigens, which are presented in Fig. 7.

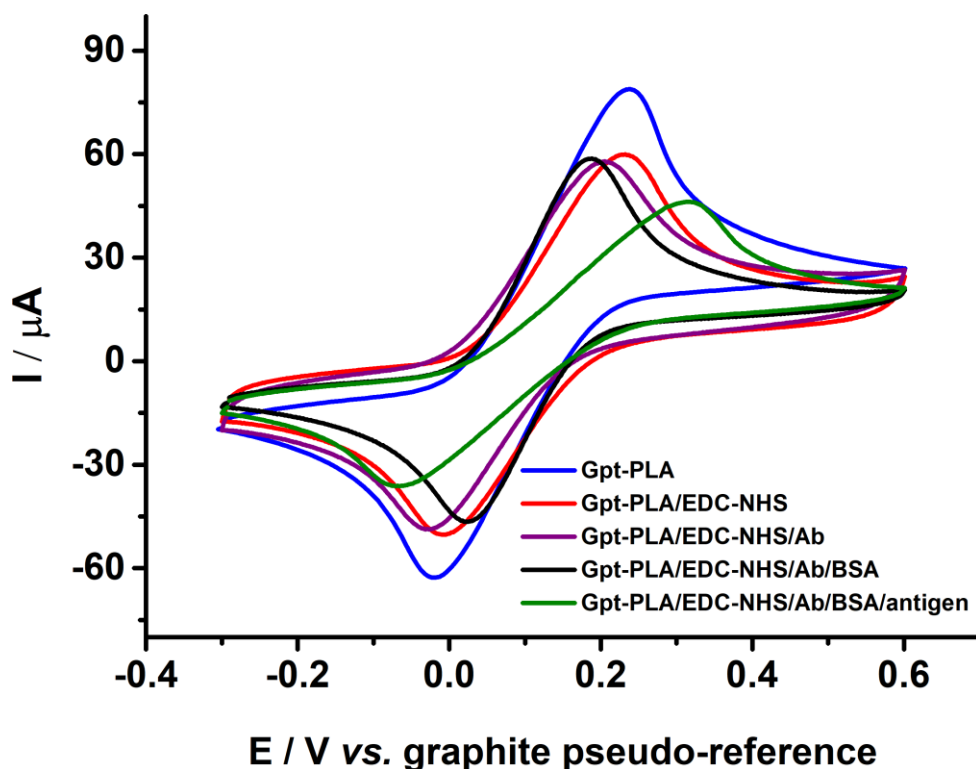


Figure 7. Cyclic voltammetric recordings in presence of 1.0 mmol L^{-1} FcMeOH in 0.1 mol L^{-1} KCl after each immobilization step. Scan rate: 100 mV s^{-1} .

It is possible to observe that, initially, both oxidation and reduction peaks from FcMeOH are present and well defined, and provide high peak current responses. The bonding of EDC-NHS provided a decrease (20%) in the current response, probably due to the hindering caused by the bound molecules onto the electrode surface. The immobilization of Ab and BSA did not affect significantly the peak current values. However, the presence of the antigen provided a significant decrease in the peak current response. Also, a decrease in the reversibility of the redox process is observed with the peak-to-peak separation. The detection of the antigen was possible due to the specific reaction of the spike protein (antigen) with the antibody bonded onto the immunosensor. The increase in the concentration of antigen provided a bulkier structure at the electrode surface, hindering the electron transfer process and, consequently, lowering the

electrochemical response of the redox probe (FcMeOH) [73]. Therefore, the drop in current peak values in the presence of the antigen attests to the proper working of the fabricated immunosensor for the detection of SARS-CoV-2 S protein.

A calibration curve for the spike protein was performed after incubation (30 min) in the presence of increasing concentrations of antigen onto the immunosensor surface. Fig. 8A presents the cyclic voltammograms obtained for 1.0 mmol L⁻¹ FcMeOH using 0.1 mol L⁻¹ KCl as the supporting electrolyte.

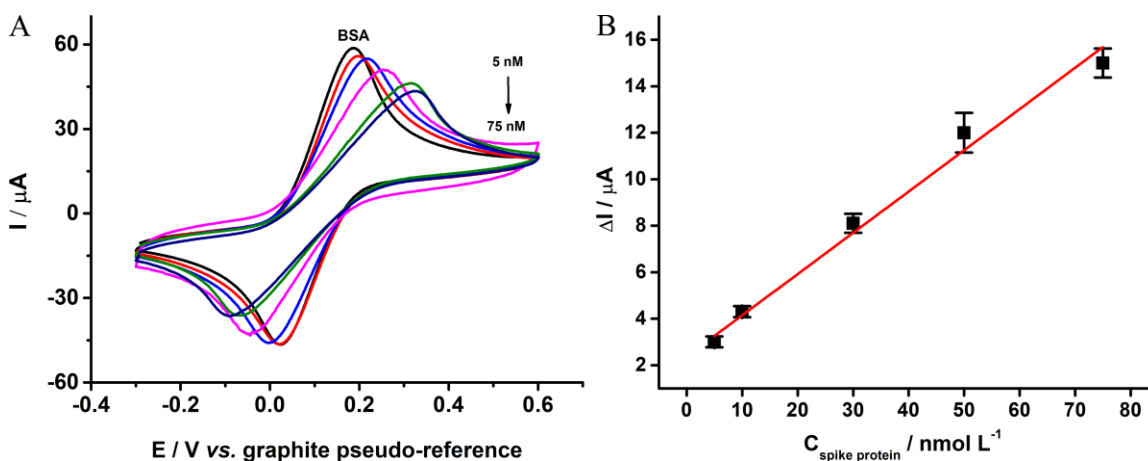


Figure 8. Cyclic voltammograms recorded in presence of 1.0 mmol L⁻¹ FcMeOH in 0.1 mol L⁻¹ KCl using the fabricated immunosensor for increasing concentrations of antigen (5.0, 10.0, 30.0, 50.0 and 75.0 nmol L⁻¹); Scan rate: 100 mV s⁻¹.

The calibration plot shown in Fig. 8B presents the relation between antigen concentration (nmol L⁻¹) and the oxidation peak current ratio between the last modification step (BSA) - analyte attachments ($\Delta\mu\text{A}$). A linear behavior was observed in a concentration range from 5.0 to 75.0 nmol L⁻¹, with a coefficient of correlation of 0.995. The LOD and LOQ obtained were calculated according to the following: $\text{LOD} = 3.3\sigma_{\text{intercept}}/s$ and $\text{LOQ} = 3 \times \text{LOD}$, where σ is the standard deviation of the intercept of

the calibration curve, and s is the sensitivity (slope) of the calibration curve. The Gpt-PLA based immunosensor provided a LOD value of 1.36 nmol L^{-1} ($0.10 \text{ } \mu\text{g mL}^{-1}$), LOQ of 4.5 nmol L^{-1} ($0.33 \text{ } \mu\text{g mL}^{-1}$), and a sensitivity of $0.17 \text{ } \mu\text{A nmol}^{-1} \text{ L}$ ($0.01 \text{ } \mu\text{A } \mu\text{g}^{-1} \text{ mL}$).

A negative control testing was performed by the incubation of a non-specific protein (BSA) in a concentration of 75.0 nmol L^{-1} ($5.74 \text{ } \mu\text{g mL}^{-1}$) for 30 min on the biosensor surface. Figure S11-A presents the cyclic voltammograms obtained for 1.0 mmol L^{-1} FcMeOH in 0.1 mol L^{-1} KCl on the biosensor without protein incubation, and after incubation of negative control (BSA) and positive control (spike protein) in the same concentration. Through Figure S11-A is possible to observe that the electrochemical response of the biosensor of the negative control is not significantly influencing, while the spike protein of the virus provides a decrease in the peak current (presenting a current response corresponding to 76% from the biosensor electrochemical signal), attesting that the biosensor is not responding to non-specific species.

To provide a demonstration that the biosensor is suitable, the analysis of the virus protein was performed in synthetic saliva by spiking ($n = 4$) with the protein in different concentrations, and incubating for 30 min. Figure S12-A presents the cyclic voltammograms obtained with the biosensor for 1.0 mmol L^{-1} FcMeOH containing 5.0, 10.0, 30.0 and 50.0 nmol L^{-1} spike protein prepared in synthetic saliva. It is possible to observe a slight change in the cyclic voltammograms profile in saliva, which probably occurred due to the complexity of the sample in comparison to the buffer solution, nevertheless, the current response is maintained, guaranteeing the analysis with adequate recovery. The recovery values were obtained (Fig. S12-B), ranging from $86.3 \pm 2.7\%$ to $96.1 \pm 10.2\%$, attesting to the suitability of the biosensor for saliva tests.

To the best of our knowledge, only two works in the literature have reported the use of 3D printed electrodes for the detection of SARS-CoV-2. Recently, Muñoz and Pumera [32] reported an interesting general approach for the bottom-up biofunctionalization of a 3D printed electrode for creating an immunosensor for COVID-19. In this work, a G-PLA 3D printed sensor was employed after a two-step surface treatment, firstly a chemical activation during 3 h using DMF was performed, followed by an electrochemical activation during 300 s in PBS solution. The assembling of the immunosensor started with the incorporation of gold nanoparticles (AuNPs) after immersion of the electrode in a HAuCl_4 solution for 1 h followed by immersion in NaBH_4 solution. Next, the electrode was immersed in cysteamine solution for 2.5 h, and then for 1 h in glutaraldehyde. The antibody was incubated for 1 h onto the aldehyde groups, and finally, the blockage with BSA during 30 min was performed, providing the final immunosensor. The authors detected the spike protein of the virus with a LOD of $0.5 \mu\text{g mL}^{-1}$, over a linear range from 1.0 to $10.0 \mu\text{g mL}^{-1}$.

A different 3D printing method was employed by Ali et al. [35] for the development of the immunosensor for COVID-19. The authors used the aerosol jet 3D printing method, creating an array of gold microcapillary electrodes, followed by the functionalization of reduced graphene oxide (rGO) nanoflakes and immobilization of the antigens. In this work, S protein was detected with a detection limit of 2.8 fmol L^{-1} . Fast responses were obtained, and sensor regeneration was possible after immersion for 1 minute in a low pH solution.

Therefore, we prove that the 3D printed electrochemical sensor obtained with the new fabricated Gpt-PLA filament can also be used successfully in biosensing. The ready-to-use platform eliminates additional steps, such as the need for surface pre-treatment. Additionally, regarding the fabrication of the immunosensor, the need for

gold nanoparticles immobilization is also dispensed, providing a simpler and functional biosensing platform with excellent analytical performance, including low limits of detection and quantification and excellent sensitivity. Thus, the versatility of the fabricated filament towards the construction of (bio)sensors was proved. In addition, the possibility of producing biosensors significantly contributes to the development of new point-of-care tests, further improving medical screening exams.

4. Conclusions

Herein, we demonstrate a simple protocol for the obtaining of a PLA-graphite-based conductive filament that enables the FDM 3D printing of innovative platforms for biosensing. Importantly, the fabricated sensors are ready-to-use and do not require time-consuming surface treatment. Moreover, the incorporation of gold nanoparticles, commonly employed for biosensor construction, is not required due to the obtained surface rich in oxygenated and carboxylate functional groups. The electrochemical performance is fantastic considering the absence of surface treatment protocols, demonstrated by the high electrochemically active surface area, fast HET, and low resistance to charge transfer. The material is very promising as it also allows the variation in material and composition of the produced filament according to the demand as well as the range of applications, with the advantage to develop structures in different designs due to 3D technology. For electrochemical (bio)sensing, the produced filaments are a great alternative for commercial ones, especially since no surface activation or pre-treatments are required, thus, reducing the amount of reagent used.

Furthermore, satisfactory detection of UA and DA was observed, presenting low LOD values (0.07 and 0.11 $\mu\text{mol L}^{-1}$, respectively). The interelectrode precision was calculated for UA detection and satisfactory results were obtained (RSD <12%, n = 5).

Moreover, recovery of 92% in the analysis of synthetic samples attested to the absence of sample matrix effects. The determination of DA was efficient in comparison to other 3D printed electrodes, and recovery values between 92 and 101% were obtained in the analysis of synthetic samples. The use of Gpt-PLA as a platform for biosensing was proved, the immunosensor fabricated was simple, involving only a few steps, and provided good sensitivity and a low LOD (1.35 nmol L^{-1}), capable of detecting SARS-CoV-2 virus at trace levels ($0.10 \mu\text{g mL}^{-1}$).

Finally, a new method for producing conductive filaments is an important knowledge base, since it allows others research groups to use it as a starting point for new academic researches, producing works of excellence using FDM 3D printing technology.

Acknowledgments

The authors are grateful to the Brazilian agencies FAPESP (2017/21097-3 and 2018/19750-3), CAPES (001), CAPES (88887.510506/2020-00 and 88887.510880/2020-00) CNPq (303338/2019-9, 427731/2018-6 and 307271/2017-0), INCTBio (CNPq grant no. 465389/2014–7) and FAPEMIG (RED-00042-16 and APQ-03141-18) for the financial support. We also acknowledge the Institute of Physics (INFIS) of the Federal University of Uberlandia for Raman (Horiba LabRAM HR Evolution Raman) spectroscopic measurements supported by the grant “Pró-Equipamentos” from the Brazilian agency CAPES and by FINEP.

References

- [1] H.H. Hamzah, S.A. Shafiee, A. Abdalla, B.A. Patel, 3D printable conductive materials for the fabrication of electrochemical sensors: A mini review,

- Electrochem. Commun. 96 (2018) 27–31.
<https://doi.org/10.1016/j.elecom.2018.09.006>.
- [2] A. Ambrosi, M. Pumera, 3D-printing technologies for electrochemical applications, Chem. Soc. Rev. 45 (2016) 2740–2755.
<https://doi.org/10.1039/c5cs00714c>.
- [3] C.W. Foster, M.P. Down, Y. Zhang, X. Ji, S.J. Rowley-Neale, G.C. Smith, P.J. Kelly, C.E. Banks, 3D Printed graphene based energy storage devices, Sci. Rep. 7 (2017) 42233. <https://doi.org/10.1038/srep42233>.
- [4] V. Katseli, A. Economou, C. Kokkinos, Single-step fabrication of an integrated 3D-printed device for electrochemical sensing applications, Electrochem. Commun. 103 (2019) 100–103. <https://doi.org/10.1016/j.elecom.2019.05.008>.
- [5] F. Novotný, V. Urbanová, J. Plutnar, M. Pumera, Preserving fine structure details and dramatically enhancing electron transfer rates in graphene 3D-printed electrodes via thermal annealing: toward nitroaromatic explosives sensing, ACS Appl. Mater. Interfaces. 11 (2019) 35371–35375.
<https://doi.org/10.1021/acsami.9b06683>.
- [6] P.L. dos Santos, V. Katic, H.C. Loureiro, M.F. dos Santos, D.P. dos Santos, A.L.B. Formiga, J.A. Bonacin, Enhanced performance of 3D printed graphene electrodes after electrochemical pre-treatment: Role of exposed graphene sheets, Sensors Actuators, B Chem. 281 (2019) 837–848.
<https://doi.org/10.1016/j.snb.2018.11.013>.
- [7] C. Kalinke, N.V. Neumsteir, G.D.O. Aparecido, T.V.D.B. Ferraz, P.L. Dos Santos, B.C. Janegitz, J.A. Bonacin, Comparison of activation processes for 3D printed PLA-graphene electrodes: Electrochemical properties and application for sensing of dopamine, Analyst. 145 (2020) 1207–1218.

<https://doi.org/10.1039/c9an01926j>.

- [8] R. Cardoso, S. Castro, J. Stefano, R. Muñoz, Drawing electrochemical sensors using a 3D printing pen, *J. Braz. Chem. Soc.* 31 (2020) 1764–1770. <https://doi.org/10.21577/0103-5053.20200129>.
- [9] E. Vaněčková, M. Bouša, Š. Nováková Lachmanová, J. Rathouský, M. Gál, T. Sebechlebská, V. Kolivoška, 3D printed polylactic acid/carbon black electrodes with nearly ideal electrochemical behaviour, *J. Electroanal. Chem.* 857 (2020) 113745. <https://doi.org/10.1016/j.jelechem.2019.113745>.
- [10] G.D. O’Neil, S. Ahmed, K. Halloran, J.N. Janusz, A. Rodríguez, I.M. Terrero Rodríguez, Single-step fabrication of electrochemical flow cells utilizing multi-material 3D printing, *Electrochem. Commun.* 99 (2019) 56–60. <https://doi.org/10.1016/j.elecom.2018.12.006>.
- [11] Z. Rymansaib, P. Iravani, E. Emslie, M. Medvidović-Kosanović, M. Sak-Bosnar, R. Verdejo, F. Marken, All-Polystyrene 3D-Printed Electrochemical Device with Embedded Carbon Nanofiber-Graphite-Polystyrene Composite Conductor, *Electroanalysis*. 28 (2016) 1517–1523. <https://doi.org/10.1002/elan.201600017>.
- [12] J. Giorgini Escobar, E. Vaněčková, Š. Nováková Lachmanová, F. Vivaldi, J. Heyda, J. Kubišta, V. Shestivska, P. Španěl, K. Schwarzová-Pecková, J. Rathouský, T. Sebechlebská, V. Kolivoška, The development of a fully integrated 3D printed electrochemical platform and its application to investigate the chemical reaction between carbon dioxide and hydrazine, *Electrochim. Acta*. 360 (2020) 136984. <https://doi.org/10.1016/j.electacta.2020.136984>.
- [13] E. Vaněčková, M. Bouša, V. Shestivska, J. Kubišta, P. Moreno-García, P. Broekmann, M. Rahaman, M. Zlámál, J. Heyda, M. Bernauer, T. Sebechlebská, V. Kolivoška, Electrochemical reduction of carbon dioxide on 3D printed

- electrodes, *ChemElectroChem.* 8 (2021) 2137–2149.
<https://doi.org/10.1002/celc.202100261>.
- [14] E. Vaněčková, M. Bouša, F. Vivaldi, M. Gál, J. Rathouský, V. Kolivoška, T. Sebechlebská, UV/VIS spectroelectrochemistry with 3D printed electrodes, *J. Electroanal. Chem.* 857 (2020) 113760.
<https://doi.org/10.1016/j.jelechem.2019.113760>.
- [15] E.M. Richter, D.P. Rocha, R.M. Cardoso, E.M. Keefe, C.W. Foster, R.A.A. Munoz, C.E. Banks, Complete additively manufactured (3D-printed) electrochemical sensing platform, *Anal. Chem.* 91 (2019) 12844–12851.
<https://doi.org/10.1021/acs.analchem.9b02573>.
- [16] R. Gusmão, M.P. Browne, Z. Sofer, M. Pumera, The capacitance and electron transfer of 3D-printed graphene electrodes are dramatically influenced by the type of solvent used for pre-treatment, *Electrochem. Commun.* 102 (2019) 83–88. <https://doi.org/10.1016/j.elecom.2019.04.004>.
- [17] V.A.O.P. Silva, W.S. Fernandes-Junior, D.P. Rocha, J.S. Stefano, R.A.A. Munoz, J.A. Bonacin, B.C. Janegitz, 3D-printed reduced graphene oxide/polylactic acid electrodes: A new prototyped platform for sensing and biosensing applications, *Biosens. Bioelectron.* 170 (2020). <https://doi.org/10.1016/j.bios.2020.112684>.
- [18] R.M. Cardoso, D.M.H. Mendonça, W.P. Silva, M.N.T. Silva, E. Nossol, R.A.B. da Silva, E.M. Richter, R.A.A. Muñoz, 3D printing for electroanalysis: From multiuse electrochemical cells to sensors, *Anal. Chim. Acta.* 1033 (2018) 49–57.
<https://doi.org/10.1016/j.aca.2018.06.021>.
- [19] M.P. Browne, F. Novotný, Z. Sofer, M. Pumera, 3D printed graphene electrodes' electrochemical activation, *ACS Appl. Mater. Interfaces.* 10 (2018) 40294–40301. <https://doi.org/10.1021/acsami.8b14701>.

- [20] C.L. Manzanares-Palenzuela, S. Hermanova, Z. Sofer, M. Pumera, Proteinase-sculptured 3D-printed graphene/polylactic acid electrodes as potential biosensing platforms: towards enzymatic modeling of 3D-printed structures, *Nanoscale*. 11 (2019) 12124–12131. <https://doi.org/10.1039/C9NR02754H>.
- [21] D.M. Wirth, M.J. Sheaff, J. V. Waldman, M.P. Symcox, H.D. Whitehead, J.D. Sharp, J.R. Doerfler, A.A. Lamar, G. Leblanc, Electrolysis activation of fused-filament-fabrication 3D-printed electrodes for electrochemical and spectroelectrochemical analysis, *Anal. Chem.* 91 (2019) 5553–5557. <https://doi.org/10.1021/acs.analchem.9b01331>.
- [22] D.P. Rocha, R.G. Rocha, S.V.F. Castro, M.A.G. Trindade, R.A.A. Munoz, E.M. Richter, L. Angnes, Posttreatment of 3D-printed surfaces for electrochemical applications: A critical review on proposed protocols, *Electrochem. Sci. Adv.* (2021) 1–15. <https://doi.org/10.1002/elsa.202100136>.
- [23] C.W. Foster, H.M. Elbardisy, M.P. Down, E.M. Keefe, G.C. Smith, C.E. Banks, Additively manufactured graphitic electrochemical sensing platforms, *Chem. Eng. J.* 381 (2020) 122343. <https://doi.org/10.1016/j.cej.2019.122343>.
- [24] M.A. Cruz, S. Ye, M.J. Kim, C. Reyes, F. Yang, P.F. Flowers, B.J. Wiley, Multigram synthesis of Cu-Ag core-shell nanowires enables the production of a highly conductive polymer filament for 3D printing electronics, *Part. Part. Syst. Charact.* 35 (2018) 1700385. <https://doi.org/10.1002/ppsc.201700385>.
- [25] R.M. Cardoso, P.R.L. Silva, A.P. Lima, D.P. Rocha, T.C. Oliveira, T.M. do Prado, E.L. Fava, O. Fatibello-Filho, E.M. Richter, R.A.A. Muñoz, 3D-Printed graphene/polylactic acid electrode for bioanalysis: Biosensing of glucose and simultaneous determination of uric acid and nitrite in biological fluids, *Sensors Actuators, B Chem.* 307 (2020) 127621.

- <https://doi.org/10.1016/j.snb.2019.127621>.
- [26] A.M. López Marzo, C.C. Mayorga-Martinez, M. Pumera, 3D-printed graphene direct electron transfer enzyme biosensors, *Biosens. Bioelectron.* 151 (2020). <https://doi.org/10.1016/j.bios.2019.111980>.
- [27] C.L. Manzanares-Palenzuela, S. Hermanova, Z. Sofer, M. Pumera, Proteinase-sculptured 3D-printed graphene/polylactic acid electrodes as potential biosensing platforms: Towards enzymatic modeling of 3D-printed structures, *Nanoscale*. 11 (2019) 12124–12131. <https://doi.org/10.1039/c9nr02754h>.
- [28] G. Martins, J.L. Gogola, L.H. Budni, B.C. Janegitz, L.H. Marcolino-Junior, M.F. Bergamini, 3D-printed electrode as a new platform for electrochemical immunosensors for virus detection, *Anal. Chim. Acta*. 1147 (2021) 30–37. <https://doi.org/10.1016/j.aca.2020.12.014>.
- [29] C. Wu, X. Chen, Y. Cai, J. Xia, X. Zhou, S. Xu, H. Huang, L. Zhang, X. Zhou, C. Du, Y. Zhang, J. Song, S. Wang, Y. Chao, Z. Yang, J. Xu, X. Zhou, D. Chen, W. Xiong, L. Xu, F. Zhou, J. Jiang, C. Bai, J. Zheng, Y. Song, Risk factors associated with acute respiratory distress syndrome and death in patients with coronavirus disease 2019 pneumonia in Wuhan, China, *JAMA Intern. Med.* 180 (2020) 934–943. <https://doi.org/10.1001/jamainternmed.2020.0994>.
- [30] Y. Wang, J. Luo, J. Liu, X. Li, Z. Kong, H. Jin, X. Cai, Electrochemical integrated paper-based immunosensor modified with multi-walled carbon nanotubes nanocomposites for point-of-care testing of 17 β -estradiol, *Biosens. Bioelectron.* 107 (2018) 47–53. <https://doi.org/10.1016/j.bios.2018.02.012>.
- [31] L.C. Brazaca, P.L. dos Santos, P.R. de Oliveira, D.P. Rocha, J.S. Stefano, C. Kalinke, R.A. Abarza Muñoz, J.A. Bonacin, B.C. Janegitz, E. Carrilho, Biosensing strategies for the electrochemical detection of viruses and viral

- diseases – A review, *Anal. Chim. Acta.* 1159 (2021) 338384.
<https://doi.org/10.1016/j.aca.2021.338384>.
- [32] J. Muñoz, M. Pumera, 3D-Printed COVID-19 immunosensors with electronic readout, *Chem. Eng. J.* 425 (2021) 131433.
<https://doi.org/10.1016/J.CEJ.2021.131433>.
- [33] A. Nazir, A. Azhar, U. Nazir, Y.F. Liu, W.S. Qureshi, J.E. Chen, E. Alanazi, The rise of 3D Printing entangled with smart computer aided design during COVID-19 era, *J. Manuf. Syst.* (2020). <https://doi.org/10.1016/j.jmsy.2020.10.009>.
- [34] Y.Y.C. Choong, H.W. Tan, D.C. Patel, W.T.N. Choong, C.-H. Chen, H.Y. Low, M.J. Tan, C.D. Patel, C.K. Chua, The global rise of 3D printing during the COVID-19 pandemic, *Nat. Rev. Mater.* 5 (2020) 637–639.
<https://doi.org/10.1038/s41578-020-00234-3>.
- [35] M.A. Ali, C. Hu, S. Jahan, B. Yuan, M.S. Saleh, E. Ju, S.J. Gao, R. Panat, Sensing of COVID-19 Antibodies in Seconds via Aerosol Jet Nanoprinted Reduced-Graphene-Oxide-Coated 3D Electrodes, *Adv. Mater.* (2020) 2006647.
<https://doi.org/10.1002/adma.202006647>.
- [36] L.P. Caetano, A.P. Lima, T.F. Tormin, E.M. Richter, F.S. Espindola, F. V Botelho, R.A.A. Munoz, Carbon-nanotube modified screen-printed electrode for the simultaneous determination of nitrite and uric acid in biological fluids using batch-injection amperometric detection, *Electroanalysis*. 30 (2018) 1870–1879.
<https://doi.org/10.1002/elan.201800189>.
- [37] S. Ku, S. Palanisamy, S.M. Chen, Highly selective dopamine electrochemical sensor based on electrochemically pretreated graphite and nafion composite modified screen printed carbon electrode, *J. Colloid Interface Sci.* 411 (2013) 182–186. <https://doi.org/10.1016/j.jcis.2013.08.029>.

- [38] T. Brooks, C.W. Keevil, A simple artificial urine for the growth of urinary pathogens, *Lett. Appl. Microbiol.* 24 (1997) 203–206.
<https://doi.org/10.1046/j.1472-765X.1997.00378.x>.
- [39] D.E. Romonti, A. V. Gomez Sanchez, I. Milošev, I. Demetrescu, S. Ceré, Effect of anodization on the surface characteristics and electrochemical behaviour of zirconium in artificial saliva, *Mater. Sci. Eng. C.* 62 (2016) 458–466.
<https://doi.org/10.1016/j.msec.2016.01.079>.
- [40] R.G. Rocha, R.M. Cardoso, P.J. Zambiasi, S.V.F. Castro, T.V.B. Ferraz, G. de O. Aparecido, J.A. Bonacin, R.A.A. Munoz, E.M. Richter, Production of 3D-printed disposable electrochemical sensors for glucose detection using a conductive filament modified with nickel microparticles, *Anal. Chim. Acta.* 1132 (2020) 1–9. <https://doi.org/10.1016/j.aca.2020.07.028>.
- [41] V.A.O.P. da Silva, V.A.P. Tartare, C. Kalinke, P.R. de Oliveira, D.C. de Souza, J.A. Bonacin, B.C. Janegitz, Lab-made 3D-printed contact angle measurement adjustable holder, *Quim. Nova.* 43 (2020) 1312–1319.
<https://doi.org/10.21577/0100-4042.20170624>.
- [42] K. Gnanasekaran, T. Heijmans, S. van Bennekom, H. Woldhuis, S. Wijnia, G. de With, H. Friedrich, 3D printing of CNT- and graphene-based conductive polymer nanocomposites by fused deposition modeling, *Appl. Mater. Today.* 9 (2017) 21–28. <https://doi.org/10.1016/j.apmt.2017.04.003>.
- [43] F. Signori, M.B. Coltelli, S. Bronco, Thermal degradation of poly(lactic acid) (PLA) and poly(butylene adipate-co-terephthalate) (PBAT) and their blends upon melt processing, *Polym. Degrad. Stab.* 94 (2009) 74–82.
<https://doi.org/10.1016/j.polymdegradstab.2008.10.004>.
- [44] I.H. Kim, Y.G. Jeong, Polylactide/exfoliated graphite nanocomposites with

- enhanced thermal stability, mechanical modulus, and electrical conductivity, *J. Polym. Sci. Part B Polym. Phys.* 48 (2010) 850–858. <https://doi.org/10.1002/polb.21956>.
- [45] L.G. Cançado, M.A. Pimenta, B.R.A. Neves, M.S.S. Dantas, A. Jorio, Influence of the atomic structure on the Raman spectra of graphite edges, *Phys. Rev. Lett.* 93 (2004) 247401. <https://doi.org/10.1103/PhysRevLett.93.247401>.
- [46] P.L. dos Santos, R.A. Timm, L.T. Kubota, J.A. Bonacin, Modulation of electrochemical properties of graphene oxide by photochemical reduction using UV-light emitting diodes, *ChemistrySelect.* 1 (2016) 1168–1175. <https://doi.org/10.1002/slct.201600121>.
- [47] S. Reich, C. Thomsen, Raman spectroscopy of graphite, *Philos. Trans. R. Soc. London. Ser. A Math. Phys. Eng. Sci.* 362 (2004) 2271–2288. <https://doi.org/10.1098/rsta.2004.1454>.
- [48] Y.-X. Weng, Y.-J. Jin, Q.-Y. Meng, L. Wang, M. Zhang, Y.-Z. Wang, Biodegradation behavior of poly(butylene adipate-co-terephthalate) (PBAT), poly(lactic acid) (PLA), and their blend under soil conditions, *Polym. Test.* 32 (2013) 918–926. <https://doi.org/10.1016/j.polymertesting.2013.05.001>.
- [49] V. Țucureanu, A. Matei, A.M. Avram, FTIR spectroscopy for carbon family study, *Crit. Rev. Anal. Chem.* 46 (2016) 502–520. <https://doi.org/10.1080/10408347.2016.1157013>.
- [50] M.D.P. Lavin-Lopez, A. Romero, J. Garrido, L. Sanchez-Silva, J.L. Valverde, Influence of different improved hummers method modifications on the characteristics of graphite oxide in order to make a more easily scalable method, *Ind. Eng. Chem. Res.* 55 (2016) 12836–12847. <https://doi.org/10.1021/acs.iecr.6b03533>.

- [51] L.A. Layqah, S. Eissa, An electrochemical immunosensor for the corona virus associated with the Middle East respiratory syndrome using an array of gold nanoparticle-modified carbon electrodes, *Microchim. Acta.* 186 (2019). <https://doi.org/10.1007/s00604-019-3345-5>.
- [52] L.C. Brazaca, J.R. Moreto, A. Martín, F. Tehrani, J. Wang, V. Zucolotto, Colorimetric paper-based immunosensor for simultaneous determination of fetuin B and clusterin toward early Alzheimer's diagnosis, *ACS Nano.* 13 (2019) 13325–13332. <https://doi.org/10.1021/acsnano.9b06571>.
- [53] I. Krupa, I. Chodák, Physical properties of thermoplastic/graphite composites, *Eur. Polym. J.* 37 (2001) 2159–2168. [https://doi.org/10.1016/S0014-3057\(01\)00115-X](https://doi.org/10.1016/S0014-3057(01)00115-X).
- [54] J.R. Camargo, I.A.A. Andreotti, C. Kalinke, J.M. Henrique, J.A. Bonacin, B.C. Janegitz, Waterproof paper as a new substrate to construct a disposable sensor for the electrochemical determination of paracetamol and melatonin, *Talanta.* 208 (2020) 120458. <https://doi.org/10.1016/j.talanta.2019.120458>.
- [55] C. Kalinke, N.V. Neumsteir, G. de O. Aparecido, T.V.D.B. Ferraz, P.L. dos Santos, B.C. Janegitz, J.A. Bonacin, No Title, *Analyst.* 145 (2020) 1207–1218. <https://pubs.rsc.org/en/content/articlehtml/2020/an/c9an01926j> (accessed September 24, 2020).
- [56] E.P. Randviir, A cross examination of electron transfer rate constants for carbon screen-printed electrodes using electrochemical impedance spectroscopy and cyclic voltammetry, *Electrochim. Acta.* 286 (2018) 179–186. <https://doi.org/10.1016/j.electacta.2018.08.021>.
- [57] J.S. Stefano, A. Paula De Lima, R.H.O. Montes, E.M. Richter, R.A.A. Muñoz, Fast determination of naproxen in pharmaceutical formulations by batch injection

- analysis with pulsed amperometric detection, *J. Braz. Chem. Soc.* 23 (2012) 1834–1838. <https://doi.org/10.1590/S0103-50532012005000055>.
- [58] F.M. Rabboh, G.D. O’Neil, Voltammetric pH measurements in unadulterated foodstuffs, urine, and serum with 3D-printed graphene/poly(lactic acid) electrodes, *Anal. Chem.* 92 (2020) 14999–15006. <https://doi.org/10.1021/acs.analchem.0c02902>.
- [59] L. Chen, E. Kätelhön, R.G. Compton, Unscrambling illusory inhibition and catalysis in nanoparticle electrochemistry: Experiment and theory, *Appl. Mater. Today*. 16 (2019) 141–145. <https://doi.org/10.1016/j.apmt.2019.05.002>.
- [60] C. Amatore, N. Da Mota, C. Sella, L. Thouin, Theory and experiments of transport at channel microband electrodes under laminar flows. 1. Steady-state regimes at a single electrode, *Anal. Chem.* 79 (2007) 8502–8510. <https://doi.org/10.1021/ac070971y>.
- [61] R.S. Nicholson, Theory and application of cyclic voltammetry for measurement of electrode reaction kinetics, *Anal. Chem.* 37 (1965) 1351–1355. <https://doi.org/10.1021/ac60230a016>.
- [62] E.P. Randviir, C.E. Banks, Electrochemical impedance spectroscopy: an overview of bioanalytical applications, *Anal. Methods*. 5 (2013) 1098. <https://doi.org/10.1039/c3ay26476a>.
- [63] D.A.C. Brownson, P.J. Kelly, C.E. Banks, In situ electrochemical characterisation of graphene and various carbon-based electrode materials: An internal standard approach, *RSC Adv.* 5 (2015) 37281–37286. <https://doi.org/10.1039/c5ra03049h>.
- [64] I. Peluso, A. Raguzzini, Salivary and urinary total antioxidant capacity as biomarkers of oxidative stress in humans, *Patholog. Res. Int.* 2016 (2016).

<https://doi.org/10.1155/2016/5480267>.

- [65] A.A. Ejaz, B. Dass, V. Lingegowda, M. Shimada, T.M. Beaver, N.I. Ejaz, A.S. Abouhamze, R.J. Johnson, Effect of uric acid lowering therapy on the prevention of acute kidney injury in cardiovascular surgery, *Int. Urol. Nephrol.* 45 (2013) 449–458. <https://doi.org/10.1007/s11255-012-0192-2>.
- [66] E.H.Z. Ho, A. Ambrosi, M. Pumera, Additive manufacturing of electrochemical interfaces: Simultaneous detection of biomarkers, *Appl. Mater. Today.* 12 (2018) 43–50. <https://doi.org/10.1016/j.apmt.2018.03.008>.
- [67] E.L. Rossini, M.I. Milani, E. Carrilho, L. Pezza, H.R. Pezza, Simultaneous determination of renal function biomarkers in urine using a validated paper-based microfluidic analytical device, *Anal. Chim. Acta.* 997 (2018) 16–23. <https://doi.org/10.1016/j.aca.2017.10.018>.
- [68] J. Ballesta-Claver, I.F. Díaz Ortega, M.C. Valencia-Mirón, L.F. Capitán-Vallvey, Disposable luminol copolymer-based biosensor for uric acid in urine, *Anal. Chim. Acta.* 702 (2011) 254–261. <https://doi.org/10.1016/j.aca.2011.06.054>.
- [69] J.F. Guan, J. Zou, Y.P. Liu, X.Y. Jiang, J.G. Yu, Hybrid carbon nanotubes modified glassy carbon electrode for selective, sensitive and simultaneous detection of dopamine and uric acid, *Ecotoxicol. Environ. Saf.* 201 (2020) 110872. <https://doi.org/10.1016/j.ecoenv.2020.110872>.
- [70] V. Mani, M. Govindasamy, S.M. Chen, R. Karthik, S.T. Huang, Determination of dopamine using a glassy carbon electrode modified with a graphene and carbon nanotube hybrid decorated with molybdenum disulfide flowers, *Microchim. Acta.* 183 (2016) 2267–2275. <https://doi.org/10.1007/s00604-016-1864-x>.
- [71] L.O. Orzari, R. Cristina de Freitas, I. Aparecida de Araujo Andreotti, A. Gatti, B.C. Janegitz, A novel disposable self-adhesive inked paper device for

- electrochemical sensing of dopamine and serotonin neurotransmitters and biosensing of glucose, *Biosens. Bioelectron.* 138 (2019) 111310. <https://doi.org/10.1016/j.bios.2019.05.015>.
- [72] J.E. Contreras-Naranjo, V.H. Perez-Gonzalez, M.A. Mata-Gómez, O. Aguilar, 3D-printed hybrid-carbon-based electrodes for electroanalytical sensing applications, *Electrochem. Commun.* 130 (2021) 107098. <https://doi.org/10.1016/j.elecom.2021.107098>.
- [73] T. Beduk, D. Beduk, J.I. de Oliveira Filho, F. Zihnioglu, C. Cicek, R. Serto, B. Arda, T. Goksel, K. Turhan, K.N. Salama, S. Timur, Rapid point-of-care COVID-19 diagnosis with a gold-nanoarchitecture-assisted laser-scribed graphene biosensor, *Anal. Chem.* 93 (2021) 8585–8594. <https://doi.org/10.1021/acs.analchem.1c01444>.
- [74] S. Sam, L. Touahir, J. Salvador Andresa, P. Allongue, J.-N. Chazalviel, A.C. Gouget-Laemmel, C. Henry de Villeneuve, A. Moraillon, F. Ozanam, N. Gabouze, S. Djebbar, Semiquantitative Study of the EDC/NHS Activation of Acid Terminal Groups at Modified Porous Silicon Surfaces, *Langmuir*. 26 (2010) 809–814. <https://doi.org/10.1021/la902220a>.